

Material Matters™

Volume 11, Number 2

ALDRICH
Materials Science

Three-dimensional Science

Printing the Future in Multiple Dimensions

3D PRINTING GRAPHENE INK:

CREATING ELECTRONIC AND BIOMEDICAL STRUCTURES
AND DEVICES

BIOPRINTING

FOR TISSUE ENGINEERING AND REGENERATIVE MEDICINE

3D AND 4D PRINTING TECHNOLOGIES:

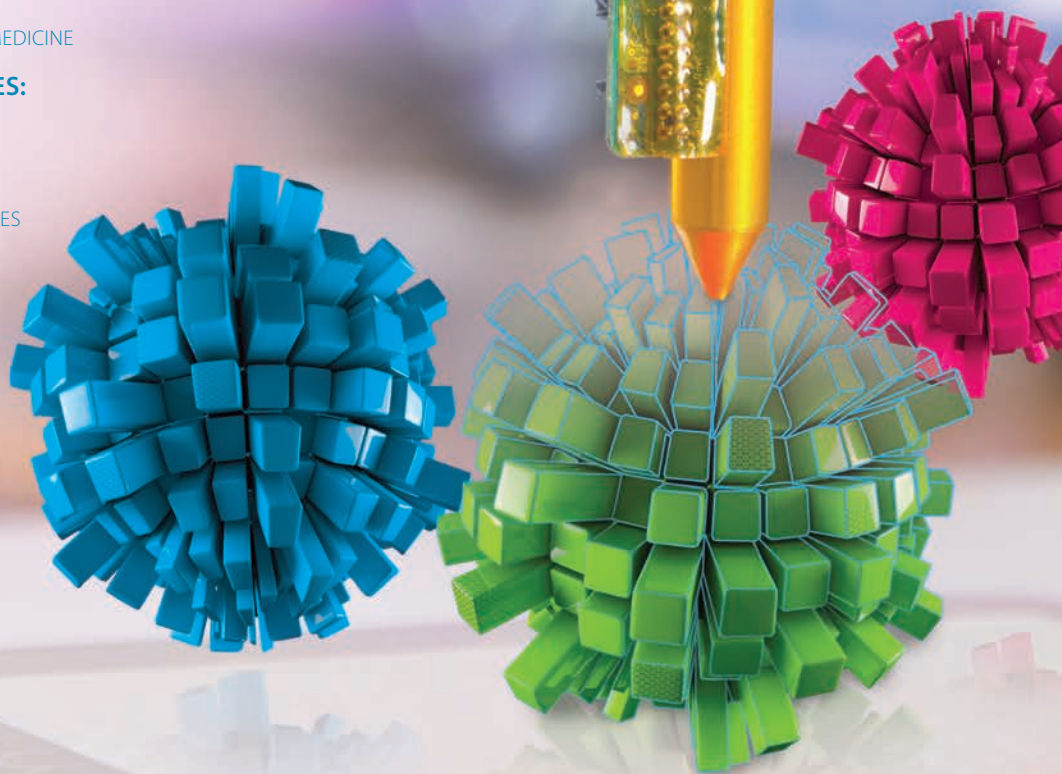
AN OVERVIEW

3D PRINTABLE CONDUCTIVE NANOCOMPOSITES

OF PLA AND MULTI-WALLED CARBON NANOTUBES

NANOPARTICLE-BASED ZINC OXIDE ELECTRON TRANSPORT LAYERS

FOR PRINTED ORGANIC PHOTODETECTORS



Introduction

Welcome to the second issue of *Material Matters*™ for 2016, focusing on multi-dimensional printing technologies and printing materials.

A number of dramatic technological innovations have added a great deal of character and dimension to the rapidly developing story of three-dimensional (3D) printing technologies. Seemingly all at once, new printing technologies have the potential to change everything from daily life to the global economy. Various two-dimensional (2D) printing techniques like inkjet and screen printing are already being used for the fabrication of flexible electronic devices. 3D printing is rapidly emerging to attract interest from both the academic community and the business world. Numerous studies have been performed to improve the methods and instrumentation for 3D printing using a wide range of new and existing materials, including plastic, metal, ceramic, wood, nanomaterials (like graphene), and even biomaterials. In this issue of *Material Matters*, we concentrate on recent advances in multi-dimensional printing technologies, from 2D to 4D, and the promising applications employing these printing techniques in multiple disciplines.

In our first article, Prof. Ramille N. Shah et al. (Northwestern University, USA) highlight novel graphene inks for 2D and 3D printing. Developments in 2D and 3D-printable graphene-based materials began with the development of ready-to-use graphene materials for device research and engineering. The authors demonstrate that their 3D graphene ink can be used to print large, robust 3D structures containing 60–70% graphene and exhibit unique mechanical and biological properties.

Prof. Peter Yang et al. (Stanford University, USA), in the second article, review the use of bioprinting for tissue engineering and regenerative medicine. Bioprinting is a new biofabrication technology used to create cellular constructs through the printing of polymer, ceramic, or other scaffolds, or even through the printing of the cells themselves. An increasing demand for new disease models, more predictive toxicity screening methods, and the emerging potential of tissue and organ printing is stimulating the development of bioprinting. The article introduces bioprinting approaches based on materials and discusses the current challenges, potential solutions, and bioprinting trends.

In the third article, Dr. Wonjin Jo et al. (Korea Institute of Science and Technology, South Korea) provide a brief overview of multi-dimensional printing technologies. The authors highlight recent advances in printing processes and printing materials development for 3D printing. They also introduce the concept of “4D printing” in which the form or function of a printed structure changes with time in response to stimuli such as temperature, light, or pressure.

Prof. Daniel Therriault et al. (École Polytechnique Montréal, Canada) discuss the promises offered by nanomaterial-based nanocomposites in the fourth article. The authors specifically focus on conductive carbon nanotubes and polymer nanocomposites for 3D printing. This research shows the strong potential for 3D printing as a novel method for manufacturing nanocomposites with promising applications such as reinforced structural parts, flexible electronics, electromagnetic shielding grids, and liquid sensors.

The final article by Dr. Gerardo Hernandez-Sosa et al. (Karlsruher Institut für Technologie, Germany) describes printed organic photodiodes which utilize ZnO nanoparticle-based electron transfer layers. The organic photodiodes featured in the article were fabricated by inkjet or aerosol printing of active organic materials and ZnO nanoparticle inks. The authors point out that using nanoparticles instead of sol-gel precursor-based layer depositions offers significant processability advantages for the manufacture of ideal flexible printed electronics.

Each article in this publication is accompanied by a list of relevant materials available from Aldrich® Materials Science. For additional product information, visit us at aldrich.com/matsci. As always, please bother us with your new product suggestions as well as thoughts and comments for *Material Matters*™ at matsci@sial.com.

About Our Cover

Three-dimensional (3D) printing is the process of creating a 3D object from a digital file. There is currently intense innovation and energy focused on 3D printing, making it an area worthy of attention and investment for many years to come. New approaches are continually being introduced that facilitate faster printing with higher resolution and using a wider array of materials, allowing advancement in many areas of research. The cover art for this issue expresses 3D printing, providing new design freedom to shape the future.



Jia Choi, Ph.D.
Aldrich Materials Science

Material Matters™

Vol. 11, No. 2

Aldrich Materials Science
Sigma-Aldrich Co. LLC
6000 N. Teutonia Ave.
Milwaukee, WI 53209, USA

To Place Orders

Telephone 800-325-3010 (USA)
FAX 800-325-5052 (USA)

International customers, contact your local Sigma-Aldrich office (sigma-aldrich.com/worldwide-offices).

Customer & Technical Services

Customer Inquiries	800-325-3010
Technical Service	800-325-5832
SAFC®	800-244-1173
Custom Synthesis	800-244-1173
Flavors & Fragrances	800-227-4563
International	314-771-5765
24-Hour Emergency	314-776-6555
Safety Information	sigma-aldrich.com/safetycenter
Website	sigma-aldrich.com
Email	aldrich@sial.com

Subscriptions

Request your FREE subscription to *Material Matters*:

Phone	800-325-3010 (USA)
Mail	Attn: Marketing Communications Aldrich Chemical Co., Inc Sigma-Aldrich Co. LLC P.O. Box 2060 Milwaukee, WI 53201-2060
Website	aldrich.com/mm
Email	sams-usa@sial.com

Online Versions

Explore previous editions
of *Material Matters* aldrich.com/materialmatters



Available for your iPad®
aldrich.com/mm

Material Matters (ISSN 1933–9631) is a publication of Aldrich Chemical Co. LLC. Aldrich is a member of the Sigma-Aldrich Group.

©2016 Sigma-Aldrich Co. LLC. All rights reserved. SIGMA, SAFC, SIGMA-ALDRICH, ALDRICH and SUPELCO are trademarks of Sigma-Aldrich Co. LLC, registered in the US and other countries. *Material Matters* is a trademark of Sigma-Aldrich Co. LLC. CastSolid, FlexSolid, MS Resin, PET+ and Vorex are registered trademarks of MadeSolid, Inc. Lactel is a registered trademark of Durect Corp. Dyesol is a registered trademark of Dyesol Ltd. iPad is a registered trademark of Apple Inc. Plexazym is a registered trademark of Röhm GmbH & Co. KG. Plexcore is a registered trademark of Plextronics, Inc. RADIANT is a registered trademark of Bio-Rad Laboratories, Inc. RESOMER is a registered trademark of Evonik Röhm GmbH. SWEiNT is a registered trademark of Chasm Advanced Materials. Xerox is a registered trademark of Xerox Corporation. CoMoCAT is a trademark of Chasm Advanced Materials. 3DXMax, 3DXNano, 3DXTech and iOn are trademarks of 3DXTech. IsoNanotubes-M, IsoNanotubes-S, PureTubes and SuperPureTubes are trademarks of NanoIntegrus, Inc. Orgacon is a trademark of Agfa-Gevaert N.V. V2V is a trademark of Chasm Technologies, Inc. Sigma-Aldrich, Sigma, Aldrich, Supelco, and SAFC brand products are sold by affiliated Sigma-Aldrich distributors. Purchaser must determine the suitability of the product(s) for their particular use. Additional terms and conditions may apply. Please see product information on the Sigma-Aldrich website at www.sigmaaldrich.com and/or on the reverse side of the invoice or packing slip. Sigma-Aldrich Corp. is a subsidiary of Merck KGaA, Darmstadt, Germany.

Table of Contents

Articles

3D Printing Graphene Ink: Creating Electronic and Biomedical Structures and Devices	41
Bioprinting for Tissue Engineering and Regenerative Medicine	49
3D and 4D Printing Technologies: An Overview	56
3D Printable Conductive Nanocomposites of PLA and Multi-walled Carbon Nanotubes	61
Nanoparticle-based Zinc Oxide Electron Transport Layers for Printed Organic Photodetectors	67

Featured Products

3D Printable Graphene Ink A list of Graphene inks for 3D printing	46
Nanocarbon Inks for Printing A list of graphene and CNT inks	46
Graphene A list of graphene, graphene nanoplatelets and graphene nanoribbons	47
Reduced Graphene Oxide A list of RGO materials	47
Graphene Oxide A list of GO materials	47
Graphene Nanocomposites A selection of graphene and reduced graphene oxide based nanocomposites	48
Biodegradable Polymers A selection of PLA, PCL, and poly(lactides) for printing	52
Poly(ethylene glycol)s (PEG) A list of PEGs for 3D printing	55
3D Printing Filaments An assortment of 3D printing filaments	59
3D Printing UV Curable Resins A selection of UV curable resins for 3D printing	60
Carbon Nanotubes A selection of single, double, multi-walled, and functionalized CNTs	64
Nanoparticle Inks for Printing A selection of ZnO, Al-doped ZnO, TiO ₂ , and Ag nanoparticle inks for printing	69
Organic Conductive Inks A list of organic conductive inks	71
Poly(3,4-ethylenedioxythiophene):poly(styrenesulfonate) (PEDOT:PSS) A list of PEDOT:PSS conductive materials	71
Polythiophene (PT) A list of PT materials	71
Fullerenes A selection of fullerenes	72
Indium Tin Oxide (ITO) Coated Substrates A selection of ITO on glass and PET substrates	72

Your Materials Matter



Bryce P. Nelson
Bryce P. Nelson, Ph.D.
Materials Science Initiative Lead

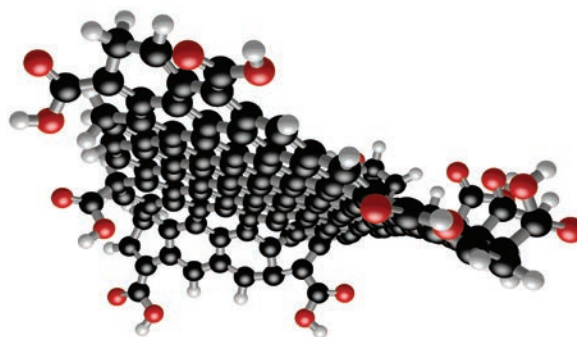
We welcome fresh product ideas. Do you have a material or compound you wish to see featured in our Materials Science line? If it is needed to accelerate your research, it matters. Send your suggestion to matsci@sial.com for consideration.

Prof. Lei Zhai of the University of Central Florida (USA) recommended the addition of edge-oxidized graphene oxide (EOGO, Aldrich Prod. No. 794341) to our catalog for use as a two-dimensional filler to improve the mechanical, thermal, and electrical properties of thermoplastics.

This few-layer graphene oxide has a high aspect ratio (1–5 nm thick and 400 nm in diameter) and high electrical conductivity, making it an effective and conductive filler. As a result, a conductive EOGO network can be created in a polymer matrix with low percolation thresholds and, therefore, with low filler loading. This is an important feature for functional composites with high electrical conductivity because composites typically become embrittled at a high filler content.^{1,2} A variety of methods including melt blending, compression/grind blending, solvent blending, and *in situ* polymerization have been used to produce EOGO/polymer composites with greatly enhanced electrical conductivity—up to 10¹² times of that of the host polymer. The enhanced performance is due to the unique EOGO structure that consists of hydroxyl and carboxyl groups on the perimeter and a non-oxidized, graphitic basal plane. This ambipolarity allows for facile dispersion of EOGO into a wide range of polymeric hosts and solvents, while preserving the useful electrical properties of few-layer graphene.

References

- (1) Du, Jinhong; Cheng, Hui-Ming. *Macromol. Chem. Phys.* **2012**, *213*, 1060–1077
- (2) Singh, Virendra; Joung, Daeha; Zhai, Lei; Das, Soumen; Khondaker, Saiful I.; Seal, Sudipta. *Prog. Mater. Sci.* **2011**, *56*(8), 1178–1271.



Graphene oxide



15–20 sheets, 4–10% edge-oxidized, 1 mg/mL, dispersion in H₂O

- Form: Brown/Black suspension
- Bulk Density: ~1.8 g/cm³
- Number of layers: 15–20

Product of Garmor Inc.

794341-50ML	50 mL
794341-200ML	200 mL

TRANSPARENT CONDUCTIVE CNT INKS

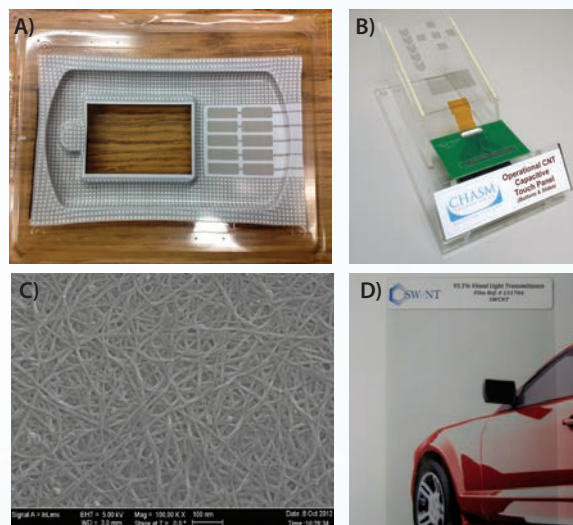
Printable • Environmentally Stable • Stretchable

Formulated using patented CoMoCAT™ CNTs, aqueous and solvent-based (V2V™) conductive inks are setting a new standard for transparent conductor performance in applications where durability and environmental stability are paramount.

V2V™: Print. Dry. Done.

Conductive CNT Ink Systems are optimized for screen printing:

- Dries quickly, evenly at low temperature
- Contains no surfactants or electrically active dispersants, binders¹
- Adheres strongly to common screen printing substrates



A) Thermoformed CNT touch sensor prototype, B) Capacitive CNT touch screen array, C) TEM scan of rod-coated CNT network (~10 mg/mm²), D) CNT TCF at 95% VLT.

SWeNT® Conductive Inks

Description	Purpose	Sheet Resistance ² (Ω/sq)			Prod. No.	
		85% VLT	90% VLT	92% VLT		
AC100	SWCNT in aqueous surfactant solution	Spray Coating	137	237	330	791490
AC200	SWCNT in aqueous surfactant solution	Meyer-Rod/Slot-Die Coating	166	251	317	791504
VC101	SWCNT in proprietary solvent system (V2V)	Screen Printing	783	1,466	2,206	792462

1. V2V inks (e.g., VC101) contain electrically inert sulfonated tetrafluoroethylene (Nafion).
2. SR measurements for AC100, 200 taken with top coat.

For detailed product information on SWeNT® Conductive Inks, visit
aldrich.com/swnt

3D PRINTING GRAPHENE INK: CREATING ELECTRONIC AND BIOMEDICAL STRUCTURES AND DEVICES



Adam E. Jakus, Ph.D.^{1,3*}, Ramille N. Shah, Ph.D.^{1,2,3}

¹Materials Science and Engineering, McCormick School of Engineering,

Northwestern University, Evanston, IL 60208 USA

²Comprehensive Transplant Center and Department of Surgery, Feinberg School of Medicine,

Northwestern University, Chicago, IL 60611 USA

³Simpson-Querrey Institute for BioNanotechnology in Medicine,

Northwestern University, Chicago, IL 60611 USA

*Email: adamjakus@gmail.com

Introduction

Since its discovery little more than a decade ago,¹ the two-dimensional (2D) allotrope of carbon—graphene—has been the subject of intense multidisciplinary research efforts. These efforts have not only revealed the exceptional electrical,² mechanical,³ thermal,⁴ and biological^{5,6} properties of graphene, but have also led to the discovery of an entire class of 2D materials with unique and potentially highly advantageous properties.⁷ As the knowledge and understanding of graphene and its properties has grown, so too has the interest in elevating this material from a scientific curiosity to a material that can be widely and readily applied to a broad range of applications and devices.

The growing interest in graphene has led to commercial efforts to produce graphene and its derivatives at scale. As a result, graphene is now available in a variety of forms, including unmodified and modified powders, films, liquid suspensions, and more. More recently, the development and availability of new, easy-to-utilize graphene-based 2D and three-dimensional (3D) printing inks^{8–10} (Prod. Nos. [798983](#), [793663](#), [796115](#), and [808156](#)) provide researchers with the necessary tools to develop and engineer graphene-based devices and applications in many areas such as flexible electronics and sensors,^{9,10} bioelectronics, and nerve, muscle, and bone tissue engineering constructs and devices.⁸

2D vs. 3D Graphene Printing Inks

It is important to distinguish between 2D inks intended for the fabrication of planar devices and 3D inks intended for the fabrication of volumetric constructs and devices (Figure 1).^{8,11,12} The rapidly emerging worldwide interest in 3D printing from consumers, researchers, and those interested in the industrial production of end-use parts has generally outpaced an adequate understanding of the underlying technologies, their uses, restrictions, and requirements, particularly 3D printing materials. This has frequently resulted in unintentional but false equivocation of established 2D printing technologies with newer 3D printing technologies and associated materials and their uses.

2D graphene inks generally make use of well-established inkjet¹⁰ and gravure-related⁹ printing hardware and processes. The 2D processes utilize 2D inks with similar requirements as those used for inkjet printing, including low viscosity (Figure 1). The need for low viscosity limits the maximum graphene content within the ink, but enables very rapid, highly precise deposition of material onto flat substrates. The resulting small or large area 2D graphene structures retain mechanical flexibility, high electrical conductivity, and thermal and chemical stability after deposition,^{9,10} making these materials exceptionally useful for a variety of current and future electronic and energy applications.

	Graphene Ink Characteristics	Deposition Characteristics	Deposited Material Cross Sections	Printed Material Characteristics
2D Ink	<ul style="list-style-type: none"> Low viscosity Moderate drying rates Extended shelf-life 	INKJET Discrete Droplets Thermo or piezo-electric driven	Substantially wets substrate (Difficult to remove from substrate)	~10 ¹ <ul style="list-style-type: none"> Extremely high electrical conductivity Mechanically flexible (if on flexible substrate)
3D Ink	<ul style="list-style-type: none"> Moderate viscosity Extremely rapid drying rates Self-supporting upon deposition Extended shelf-life 	SYRINGE EXTRUSION Room temperature Plastic or metal nozzle Continuous fibers Pneumatically or mechanically driven Extrusion Pressures = 5–800 kPa	Partially wets substrate prior to rapid drying (Easy to remove from substrate)	~10 ² –10 ³ Subsequent material can span gaps <ul style="list-style-type: none"> High electrical conductivity Mechanically flexible Highly bioactive

Figure 1. Characteristics comparison of 2D and 3D graphene inks, their deposition processes, and printed material characteristics.

Graphene has also demonstrated substantial promise for 3D materials fabrication.⁸ For example, an extensive variety of graphene-containing composite foams,¹³ hydrogels,¹⁴ and thermoplastics¹⁵ are already in use. 3D printing graphene inks are a new class of graphene materials that can be utilized to rapidly create user-defined 3D graphene structures.⁸ Unlike 2D graphene inks, which do not need to be mechanically self-supporting upon deposition onto a substrate, 3D inks must satisfy a much broader set of requirements,¹¹ such as retaining significant material functionality as well as having the ability to be printable into volumetric structures comprised of one to many thousands of layers. We have developed 3D printing inks that are printed via room-temperature extrusion from a mechanically or pneumatically driven syringe (Figure 1) in much the same way an individual uses a standard syringe to extrude material from a needle or nozzle by hand. The 3D inks and associated room-temperature extrusion 3D printing process are distinct from the widely used fused-deposition modeling (FDM) 3D printing approaches, which utilize thermoplastic filaments extruded at elevated temperatures.

3D printing graphene inks⁸ and related materials employ an evaporation driven solidification mechanism, whereby an ink is formulated by dissolving a polymer in a fast-evaporating solvent such as chloroform or dichloromethane. The ink is extruded at ambient or near ambient temperatures and rapidly solidifies as the solvent evaporates and the polymer comes out of solution. These 3D inks are user friendly, easily printable, print very rapidly, and exhibit highly advantageous functional materials properties.

3D Printing Graphene Ink Characteristics

3D printing graphene ink⁸ (Prod. No. 808156) is a moderate viscosity (25–35 Pa.s) graphene suspension comprised of graphene, dissolved elastomeric polymer binder, and a mixture of solvents that can be 3D printed (or used with any standard syringe) from a nozzle (50–2,000 μm in diameter; **Figure 2A**) under ambient conditions to rapidly create 3D graphene-based constructs that can be handled immediately (no drying time required; **Figure 2B**). The resulting 3D printed material is comprised of 60 vol.% graphene and 40 vol.% elastomeric polymer. Due to the rapid solidification of the 3D printing graphene ink, it must not be exposed to an open environment for an extended period of time when not in use. It may be possible to recover dried inks by adding a small volume of dichloromethane (Prod. Nos. 270563, 676853, 320269, and more) followed by mechanical stirring or shaking to homogenize. However, inks that are reconstituted in this way tend to suffer from more nozzle clogging events than the unreconstituted native inks. The solvent contents of the 3D inks also require that they not be exposed to materials that are soluble in dichloromethane, including polystyrene and low density polyethylene, prior to washing (more on washing in the following sections).

3D-printed Graphene Objects

A syringe-based 3D printer is not required to use the 3D printing graphene ink, although it is desirable for precision X, Y, Z spatially controlled deposition of the material. In place of a 3D printing platform, a standard hand or mechanically driven syringe may be used to extrude the 3D printing graphene inks and produce solid structures. Due to the elongated morphology of the comprising graphene flakes and shear forces from nozzle extrusion, the 3D printed graphene adopts a micro-texture defined by the lengths of the individual graphene particles aligned with, and stacked perpendicular to the fiber direction (**Figure 2D**).⁸ Fabrication of multi-layer graphene objects is done through deposition of sequential materials in a pre-defined pattern and pre-defined object geometry (**Figure 2C**). The software associated with defining internal patterns and overall object geometry varies greatly and is typically specific to individual 3D printing platforms.

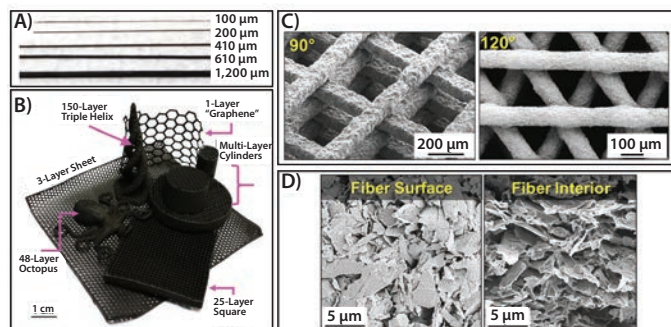


Figure 2. A) Photograph of graphene fibers extruded from nozzles with indicated diameters. Typically, the rapid drying of the 3D printing graphene ink upon deposition results in a 10% diameter reduction (i.e., Ink extruded from 100 μm tip results in ~90 μm fiber). B) Photograph of a variety of few- and many-layer graphene architectures 3D-printed from the 3D printing graphene ink using a range of nozzle diameters. C) SEM of 0–90° alternating and 0–120–240° alternating graphene structures produced from 3D printing graphene inks and extruded from 100 and 150 μm nozzles, respectively. D) Scanning electron micrograph (SEM) of surface and interior 3D-printed graphene fiber of 100 μm diameter. Modified from Reference 8.

Versatility and Handling

A 3D-printed graphene object can be physically handled immediately after production and is surprisingly robust despite the high graphene content. Residual solvents can be removed by washing objects in 70% ethanol.⁸ Few-layer objects, such as sheets, can be rolled, folded, and cut in a similar manner to standard paper (**Figure 3A**). Even thick objects can be cut or “punched” to yield many samples of defined sizes from a single 3D-printed object (**Figure 3B**). Finally, the nature of the 3D printing graphene inks enables independently 3D-printed graphene objects to be fused together to create larger and/or much more complex objects than could be 3D-printed directly (**Figure 3C**). This is achieved through conservative application of small volumes of graphene inks at contact surfaces of one or both of the parts to be joined. The freshly deposited ink locally dissolves the polymer matrix in the 3D-printed graphene and rapidly evaporates, bringing the just-dissolved polymer out of solution and creating a mechanically and electrically seamless interface between the joined objects.⁸

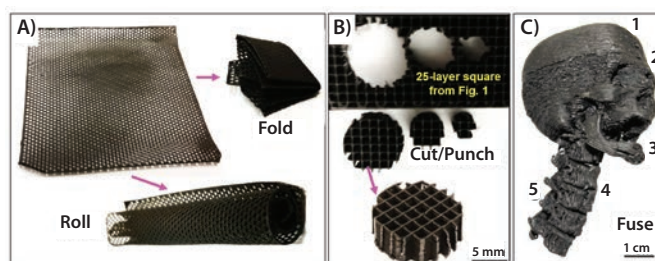


Figure 3. A) Graphene structures from 3D-printed graphene inks are flexible, and in the case of sheets (8 cm diameter), can be easily rolled, folded, cut, etc. B) Smaller graphene objects can also be directly cut or punched from larger 3D-printed graphene objects. This photo illustrates circular graphene samples punched from the 25-layer graphene square shown in **Figure 2**. C) Photograph of anatomically correct, scaled human skull, mandible, and upper spine produced by fusing five independently 3D-printed graphene parts together by lightly applying 3D printing graphene inks at points of contact.

Mechanical, Thermal, and Electrical Properties

3D-printed graphene objects derived from 3D printing graphene inks are mechanically plastic in nature (**Figure 4A,4B**),⁸ can undergo substantial strain (>80%) prior to failure, and exhibit yield and ultimate tensile strengths of less than 1 MPa. Thus, 3D-printed graphene objects are relatively soft in nature and can be shaped and modified after 3D printing to suit individual requirements. Although graphene itself is compatible with high temperatures,⁴ the elastomeric matrix (responsible for the highly versatile mechanical properties), comprising 40% of the solids volume of the material, is not. The polymer will decompose at temperatures at or above 150 °C, which causes the material to become mechanically brittle (**Figure 4B**),⁸ even though the 3D-printed architecture is maintained.

Due to the high graphene content, objects created from 3D printing graphene inks are electrically conductive, exhibiting as-printed conductivities in excess of 650 S/m, which can be improved to >870 S/m if the material is thermally annealed in air at 50 °C for approximately 30 minutes (**Figure 4C**).⁸ This is the highest recorded conductivity for a 3D-printed material that is not a metal or alloy. The nature of the ink and 3D printing process also ensures that printed layer boundaries do not act as electrical defects, which would otherwise inhibit conductivity across small and large objects.

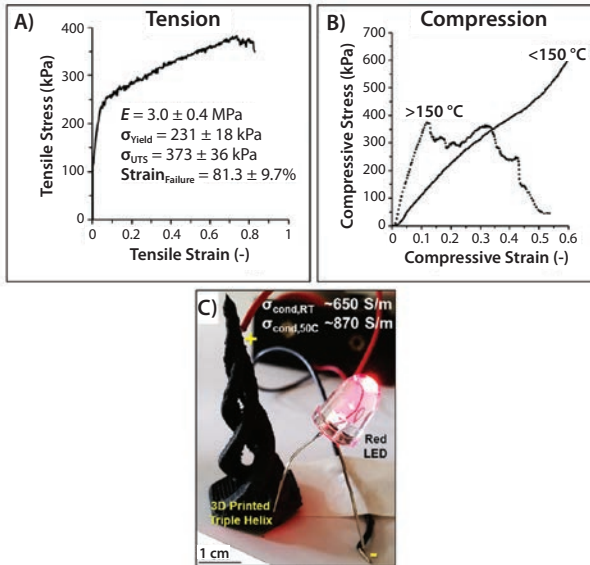


Figure 4. A) Despite the exceptionally high graphene content, 3D-printed graphene objects are relatively soft and can withstand upwards of 80% tensile strain. B) Under compression, 3D-printed graphene objects plastically deform if not previously heated to temperatures $\geq 150^\circ\text{C}$. C) Photograph illustrating electrical conductivity of a 3D-printed graphene object (triple helix shown in **Figure 2**). Adapted from Reference 8.

Biological Properties

Bioactivity and the potential of biocompatibility are the most exceptional aspects of 3D-printed graphene from 3D printing graphene inks.⁸ Once washed to remove residual solvents, 3D-printed graphene contains only graphene flakes, and a biocompatible elastomeric polymer. *In vitro* studies using bone marrow derived adult human mesenchymal stem cells (hMSCs) and cultured in standard DMEM (Dulbecco's Modified Eagle's medium) growth medium with fetal bovine serum (no biochemical, mechanical, or electrical differentiation cues) illustrate that 3D-printed graphene not only supports stem cell viability (**Figure 5A**) and proliferation over the course of at least weeks, but that the stem cells begin differentiating into glial and neuron-like cells, as indicated by both gene expression and cell morphology (**Figure 5B**).⁸ This is remarkable, and the first time a material alone (without additional biological factors) has induced such strong neurogenic behavior in adult human stem cells. Preliminary *in vivo* experiments using a BULBc mouse subcutaneous model reveal that over the course of 7 and 30 days, native tissues rapidly integrate with and vascularize the implanted 3D-printed graphene constructs (**Figure 5C–F**) with no significant immune response.⁸ Combined with its ability to be 3D-printed into nearly any form, its ability to be mechanically manipulated, its electrical conductivity, and its bioactivity, 3D-printed graphene is an excellent addition to the 3D printing biomaterials palette,¹¹ with many fundamental and translational applications on the horizon.

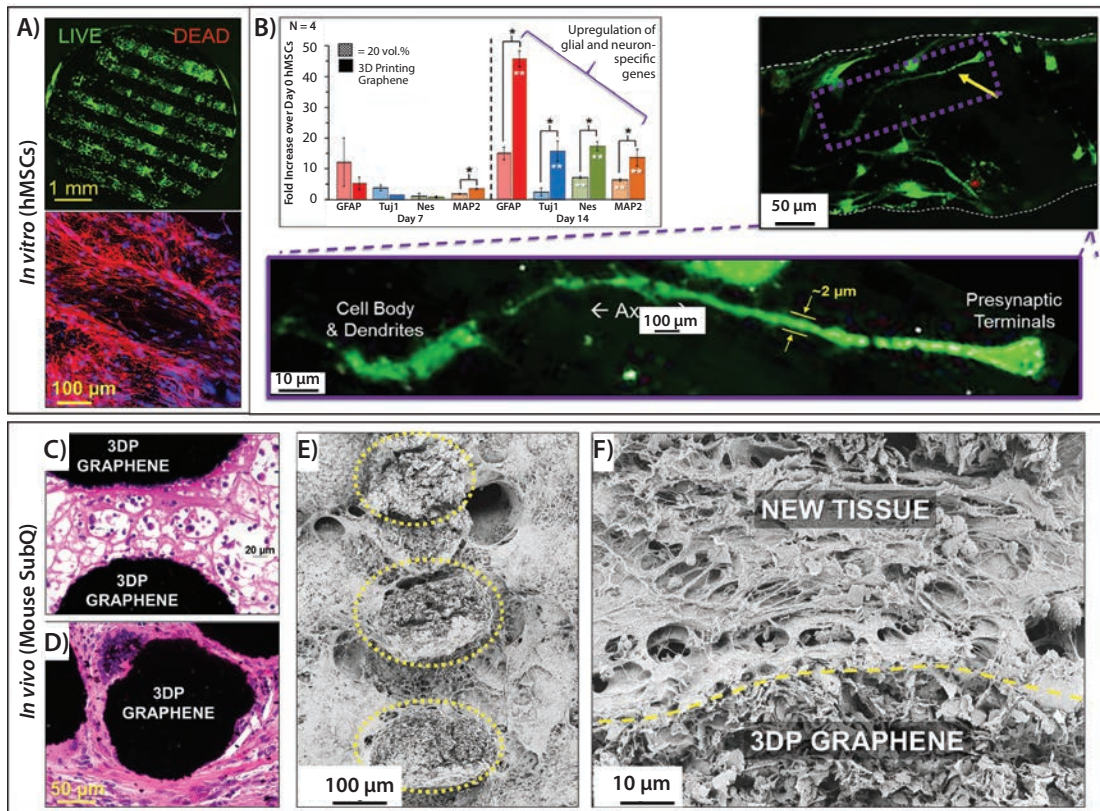


Figure 5. A) Top: Confocal microscopy reconstruction, top-down view of live (green) and dead (red) human mesenchymal stem cells on 3D-printed graphene 21 days after initial cell seeding; Bottom: confocal microscopy reconstruction showing cytoskeletal extensions (red) and cell nuclei (blue). B) Glial and neurogenic-relevant gene expression of hMSCs on 3D-printed graphene and lower content graphene material, 7 and 14 days after initial cell seeding and cultured in simple DMEM + FBS medium. Corresponding images are live/dead confocal reconstructions of hMSC derived neuron-like cells on 3D-printed graphene 14 days after initial seeding. Modified from Reference 8. C) H&E histological micrograph of 3D-printed graphene scaffold explanted 7, and D) 30 days after subcutaneous implantation into the backs of female BULBc mice. Black is the cross-section of individual 3D-printed graphene struts comprising the scaffold, pink is new cellular and extracellular tissue, and purple/blue are cell nuclei. E) SEM of 3D-printed graphene scaffold and integrated tissue 7 days after subcutaneous implantation into mice. Cross-section of comprising graphene structures, outlined by yellow dotted lines. F) SEM micrograph of day 30 explanted *in vivo* 3D-printed graphene sample showing tight interface between 3D-printed graphene material and new, integrated tissue.

Conclusions and Future Prospects

Recent developments in 2D and 3D printable graphene-based materials are beginning to bring the story of graphene full circle; from the discovery of graphene little more than decade ago, to the extensive fundamental research into its properties and their underlying mechanisms, to large-scale synthesis, to the development of ready-to-use graphene materials for device research and engineering. Based on these rapid developments and continued interest, it is safe to say that graphene materials are successfully making the transition from scientific curiosity to an indispensable tool, forming the foundation for the development of a broad array of new, advanced electronic, bioelectronics, and biomedical technologies.

Acknowledgments

The authors acknowledge the support and the use of the following facilities: Northwestern University Cell Imaging Facility supported by NCI CCSG P30 CA060553 awarded to the Robert H. Lurie Comprehensive Cancer Center; EPIC facility (NUANCE Center_Northwestern University) supported by NSF DMR-1121262 and EEC-0118025[003]; Northwestern University Mouse Histology and Phenotyping Laboratory and Cancer Center supported by NCI CA060553; and the Equipment Core Facilities at the Simpson Querrey Institute for BioNanotechnology at Northwestern University developed by support from The U.S. Army Research Office, the

U.S. Army Medical Research and Material Command, and Northwestern University. This research was also supported by Northwestern University's International Institute for Nanotechnology (NU# SP0030341), Northwestern University's McCormick Research Catalyst Award and the Office of Naval Research MURI Program (N00014-11-1-0690).

References

- (1) Novoselov, K. S.; Geim, A. K.; Morozov, S. V.; Jiang, D.; Zhang, Y.; Dubonos, S. V.; Grigorieva, I. V.; Firsov, A. A. *Science*. **2004**, *306*, 666.
- (2) Castro Neto, A. H.; Guinea, F.; Peres, N. M. R.; Novoselov, K. S.; Geim, A. K. *Rev. Mod. Phys.* **2009**, *81*, 109.
- (3) Lee, C.; Wei, X. D.; Kysar, J. W.; Hone, J. *Science*. **2008**, *321*, 385.
- (4) Balandin, A. A.; Ghosh, S.; Bao, W. Z.; Calizo, I.; Teweldebrhan, D.; Miao, F.; Lau, C. N. *Nano Lett.* **2008**, *8*, 902.
- (5) Shen, H.; Zhang, L. M.; Liu, M.; Zhang, Z. J. *Theranostics*. **2012**, *2*, 283.
- (6) Zhang, Y.; Nayak, T. R.; Hong, H.; Cai, W. B. *Nanoscale*. **2012**, *4*, 3833.
- (7) Chhowalla, M.; Shin, H. S.; Eda, G.; Li, L.-J.; Loh, K. P.; Zhang, H. *Nat. Chem.* **2013**, *5*, 263.
- (8) Jakus, A. E.; Secor, E. B.; Rutz, A. L.; Jordan, S. W.; Hersam, M. C.; Shah, R. N. *ACS Nano*. **2015**, *9*, 4636.
- (9) Secor, E. B.; Lim, S.; Zhang, H.; Frisbie, C. D.; Francis, L. F.; Hersam, M. C. *Adv. Mater.* **2014**, *26*, 4533.
- (10) Secor, E. B.; Prabhurashi, P. L.; Puntambekar, K.; Geier, M. L.; Hersam, M. C. *J. Phys. Chem. Lett.* **2013**, *4*, 1347.
- (11) Jakus, A. E.; Rutz, A. L.; Shah, R. N. *Biomed. Mater.* **2016**, *11*, 014102.
- (12) Jakus, A. E.; Taylor, S. L.; Geisendorfer, N. R.; Dunand, D. C.; Shah, R. N. *Adv. Funct. Mater.* **2015**, *25*, 6985.
- (13) Zhao, Y.; Liu, J.; Hu, Y.; Cheng, H.; Hu, C.; Jiang, C.; Jiang, L.; Cao, A.; Qu, L. *Adv. Mater.* **2013**, *25*, 591.
- (14) Chen, J.; Sheng, K.; Luo, P.; Li, C.; Shi, G. *Adv. Mater.* **2012**, *24*, 4569.
- (15) Leigh, S. J.; Bradley, R. J.; Purcell, C. P.; Billson, D. R.; Hutchins, D. A. *PLOS ONE* **2012**, *7*.

3D Printable Graphene Ink

For a complete list of available materials, visit aldrich.com/3dp.

Particle Size (µm)	Viscosity (Pa.s)	Resistivity (Ω/cm)	Prod. No.
1 - 20 (length and width) 1 - 15 (thick)	25-45 (At low shear stresses. Shear thins to ~10-15 Pa.s at Shear Stress = 100 Pa)	0.12-0.15 (as 3D-printed fibers, not ink, 200-400 µm diameter)	808156-5ML

Nanocarbon Inks for Printing

For a complete list of available materials, visit aldrich.com/inks.

Graphene Inks

Name	Particle Size	Viscosity	Resistivity	Prod. No.
Graphene dispersion, with ethyl cellulose in cyclohexanone and terpineol, inkjet printable	≤3 µm	8-15 mPa.s at 30 °C	resistivity 0.003-0.008 Ω/cm (thermally annealed 250 °C for 30 minutes, film thickness >100 nm)	793663-5ML
Graphene dispersion, with ethyl cellulose in terpineol, gravure printable	≤3 µm	0.75-3 Pa.s at 25 °C	resistivity 0.003-0.008 Ω/cm (thermally annealed 250 °C for 30 minutes, film thickness >100 nm)	796115-10ML
Graphene dispersion, with ethyl cellulose in terpineol, screen printable	≤3 µm	5-50 Pa.s at 25 °C	resistivity 0.003-0.008 Ω/cm (thermally annealed 300 °C for 30 minutes, film thickness >100 nm, 25 °C)	798983-10ML
Graphene ink in water, Inkjet printable	80-500 nm (exfoliated graphene flakes)	1 cP (100 s ⁻¹)	sheet resistance 4k Ω/sq (80 nm thickness)	808288-5ML
Graphene ink in water, flexo/gravure/screen printable	500-1,500 nm (exfoliated graphene flakes)	570 cP (100 s ⁻¹) 140 cP (1,000 s ⁻¹)	sheet resistance 10 Ω/sq (25 µm thickness)	805556-10ML
Graphene ink in water, screen printable	500-1,500 nm (exfoliated graphene flakes)	350 cP (100 s ⁻¹) 1,800 cP (1,000 s ⁻¹)	sheet resistance 10 Ω/sq (25 µm thickness)	808261-10ML

Single-walled Carbon Nanotube Inks

SWCNT Concentration	Form	Viscosity	Sheet Resistance	Prod. No.
1.00 ± 0.05 g/L (by Absorbance at 854 nm)	dispersion in H ₂ O (black liquid)	3.0 mPa.s	sheet resistance <600 Ω/sq (at 85% VLT (ohm/sq), by 4-point probe on prepared film by spray)	791504-25ML 791504-100ML
1 mg/mL	viscous liquid (black)	17.7 Pa.s at 25 °C	sheet resistance <1,000 Ω/sq (by 4-point probe on prepared, at 87.5% VLT (ohm/sq))	792462-25ML 792462-100ML
0.20 ± 0.01 g/L (by Absorbance at 854 nm)	dispersion in H ₂ O (black liquid)	~1.0 mPa.s	resistance <400 Ω/sq (by 4-point probe on prepared film by spray)	791490-25ML 791490-100ML

Graphene

For a complete list of available materials, visit aldrich.com/graphene.

Graphene and Graphene Nanoplatelets

Name	Form	Composition	Description	Prod. No.
Graphene nanoplatelets	powder	Graphene nanoplates as produced	Surfactant type: Anionic Surfactant	799084-500MG
	powder	Carbon >95 wt. % Oxygen <2 wt. %	hydrophobic	806668-25G
	powder	Carbon >85 wt. % Oxygen >3 wt. %	Dispersibility: dichloromethane, N-methyl-2-pyrrolidone, and other non-polar solvents hydrocarbon functionalized, hydrophobic	806633-25G
	powder	Carbon >95 wt. % Oxygen >1 wt. %	Dispersibility: Water, THF, DMF oxidized	806641-25G
	powder	Carbon >70 wt. % Oxygen >10 wt. %	Dispersibility: water (high stability in aqueous medium) polycarboxylate functionalized, hydrophilic	806625-25G
	dispersion in H ₂ O, 1 mg/mL	Graphene 0.1 wt. % Water 99.9 wt. %	Surfactant type: Anionic Surfactant	799092-50ML
Graphene dispersion	dispersion (in NMP), 10 mg/mL	Graphene 1 wt. % NMP 99 wt. %	dispersion in NMP	803839-5ML

Graphene Nanoribbons

Name	Purity	Dimension (L x W)	Surface Area (BET m ² /g)	Prod. No.
Graphene nanoribbons, alkyl functionalized	≥85% carbon basis, TGA	2-15 μm x 40-250 nm	38	797766-500MG
Graphene nanoribbons	≥90.0% carbon basis, TGA	2-15 μm x 40-250 nm	48-58	797774-500MG

Reduced Graphene Oxide

For a complete list of available materials, visit aldrich.com/graphene.

Description	Composition	Conductivity	Prod. No.
chemically reduced	Carbon >95 wt. % Nitrogen >5 wt. %	>600 S/m	777684-250MG 777684-500MG
chemically reduced by hydrazine	Carbon >75% Nitrogen <5%	7,111 S/m (pressed pallet)	805424-1G
amine functionalized	Carbon >65 wt. % Nitrogen >5 wt. %	-	805432-500MG
octadecylamine functionalized	Carbon >78 wt. % Nitrogen >3 wt. %	6.36 S/m (pressed pellets)	805084-500MG
tetraethylene pentamine functionalized	Carbon >65 wt. % Nitrogen >8 wt. %	-	806579-500MG
piperazine functionalized	Carbon >65 wt. % Nitrogen >5 wt. %	70.75 S/m (pressed pellets)	805440-500MG

Graphene Oxide

For a complete list of available materials, visit aldrich.com/graphene.

Name	Form	Description	Prod. No.
Graphene oxide	film	4 cm (diameter) x 12-15mm (thickness), non-conductive	798991-1EA
	powder	15-20 sheets 4-10% edge-oxidized	796034-1G
	powder or flakes	sheets	763713-250MG 763713-1G
	dispersion in H ₂ O	1 mg/mL, 15-20 sheets 4-10% edge-oxidized	794341-50ML 794341-200ML
	dispersion in H ₂ O	2 mg/mL	763705-25ML 763705-100ML
	dispersion in H ₂ O	4 mg/mL, dispersibility: Polar solvents monolayer content (measured in 0.5 mg/mL): >95%	777676-50ML 777676-200ML
	Graphene oxide nanocolloids	dispersion in H ₂ O	2 mg/mL
Graphene oxide, alkylamine functionalized	dispersion in toluene	2.0 mg/mL <0.5 % (w/w)	809055-50ML
Graphene oxide, ammonia functionalized	dispersion in H ₂ O	1 mg/mL	791520-25ML 791520-100ML

Graphene Nanocomposites

For a complete list of available materials, visit aldrich.com/graphene.

Reduced Graphene Oxide-based Nanocomposites

Name	Particle Size (nm)	Composition	Prod. No.
Fe ₃ O ₄ /reduced graphene oxide nanocomposite	5-25 (Fe ₃ O ₄ nanocrystal)	reduced graphene oxide 10-17% Fe ₃ O ₄ nanocrystal 3-8% acetone ~80%	803804-5ML
Mn ₃ O ₄ /reduced graphene oxide nanocomposite	5-25 (Mn ₃ O ₄ nanocrystal)	reduced graphene oxide 10-17% Mn ₃ O ₄ nanocrystal 3-8% acetone ~80%	803812-5ML
Pd/reduced graphene oxide nanocomposite	5-50 (Pd nanocrystal)	reduced graphene oxide 5-20% Pd nanocrystal <5% acetone ~80%	803790-5ML
Pt/reduced graphene oxide nanocomposite	2-5 (Pt nanocrystal)	reduced graphene oxide 5-20% Pt nanocrystal <5% acetone ~80 wt. %	803782-5ML
PtCo/reduced graphene oxide nanocomposite	2-5 (PtCo nanocrystal)	reduced graphene oxide 10-18% PtCo nanocrystal 2-10% acetone ~80%	803901-5ML
PtPd/reduced graphene oxide nanocomposite	5-50 (PtPd nanocrystal)	reduced graphene oxide 10-18% PtPd nanocrystal 2-10% acetone ~80%	803820-5ML

Graphene-based Nanocomposites

Name	Particle Size (nm)	Composition	Prod. No.
Fe ₃ O ₄ /graphene nanocomposite	5-25 (Fe ₃ O ₄ nanocrystal)	graphene 3-8% Fe ₃ O ₄ nanoparticle 4-9% acetone ~80 wt. %	803715-5ML
Mn ₃ O ₄ /graphene nanocomposite	5-25 (Mn ₃ O ₄ nanocrystal)	graphene 3-8% Mn ₃ O ₄ nanoparticle 4-9% acetone ~80 wt. %	803723-5ML
Pd/graphene nanocomposite	5-50 (Pd nanocrystal)	graphene 6-10% Pd nanoparticle 2-6% acetone ~80 wt. %	803707-5ML
Pt/graphene nanocomposite	2-5 (Pt nanocrystal)	graphene 6-10% Pt nanoparticle 1-4% acetone ~80 wt. %	803693-5ML
PtCo/graphene nanocomposite	2-5 (PtCo nanocrystal)	graphene 10-15% PtCo nanoparticle 5-10% acetone ~80 wt. %	803766-5ML
PtPd/graphene nanocomposite	5-50 (PtPd nanocrystal)	graphene 10-15% PtPd nanoparticle 5-10% acetone ~80 wt. %	803758-5ML

BIOPRINTING

FOR TISSUE ENGINEERING AND REGENERATIVE MEDICINE



Chi-Chun Pan,^{1,2} Arnaud Bruyas,¹ Yunzhi Peter Yang^{1,3,4}
 Departments of ¹Orthopedic Surgery, ²Mechanical Engineering,
³Materials Science and Engineering, and ⁴Bioengineering
 Stanford University, 300 Pasteur Drive, Stanford, CA 94305
 Email: ypyang@stanford.edu

Introduction

In the past two decades, tissue engineering and regenerative medicine have become important interdisciplinary fields that span biology, chemistry, engineering, and medicine.^{1,2} These new fields promote the healing and restoration of lost function in damaged or diseased tissues and organs by combining scaffolds, cells, and biological signaling molecules to recreate functional biological substitutes and mimic native tissues and functions.³ One objective of tissue engineering and regenerative medicine is the fabrication of viable tissues and organs for transplantation, but with the exceptions of thin skin and avascular cartilage,⁴ limited success in human patients has been achieved due to the complexity of tissue biology. The traditional tissue engineering approach includes loading cells onto a solid porous biomaterial, called a scaffold, in the presence or absence of growth factors that encourage cells to form the desired tissues with biomimetic complexity.⁵ However, the desired result is rarely achieved because the three component mixture does not adequately promote formation of a well-defined spatial distribution of cells, growth factors, and biomaterials at the microscale level that is characteristic of a tissue-like structure. Three-dimensional (3D) printing, also known as additive manufacturing (AM), holds great promise to overcome this limitation in tissue engineering. Because it is a layer-by-layer process, 3D printing enables the formation of complex geometries using multiple materials (Figure 1). 3D printing for tissue engineering has evolved into a new technology, called bioprinting, defined as “the use of material transfer processes for patterning and assembling biologically relevant materials, molecules, cells, tissues, and biodegradable biomaterials with a prescribed organization to accomplish one or more biological functions.”⁶ In particular, bioprinting enables personalizable

and precision medicine by engineering anatomically shaped implants with tissue-like complexity using a patient’s own cells. Currently, 3D bioprinting technologies can be classified into two categories: acellular and cellular constructs.⁷ Acellular bioprinting is used to manufacture the scaffold and biomaterial itself in the absence of cells during the printing process. Acellular bioprinting offers higher accuracy and greater shape complexity than cellular constructs because the fabrication conditions are less restrictive than methods that require maintenance of cell viability. For cellular bioprinting, cells and other biological agents are integrated into the material during manufacturing in order to fabricate living tissue constructs. It is clear that the printing parameters, biomaterials, and properties of the 3D-printed constructs are, therefore, different in each category because of the presence or absence of cells and biological substances. Here we briefly introduce and discuss these two approaches based on the suitable materials for these constructs and the fabrication processes used to manufacture them. We also discuss current limitations, potential solutions, and future directions in bioprinting.

Manufacturing of Acellular Scaffolds

An acellular scaffold consists of a porous structure that mimics the mechanical and biochemical properties of the extracellular matrix (ECM) and provides mechanical integrity as well as a template for cell attachment in order to stimulate tissue formation.⁸ Acellular scaffolds must present biocompatible and bioresorbable properties as well as biochemical, biophysical, biomechanical, bioelectrical, and biomagnetic signals.⁹ Since pores provide room for cell migration and tissue ingrowth, facilitate vasculature formation, and improve cell viability,¹⁰ porosity and porous structures are other key features for the scaffold. Thus, the use of AM is highly beneficial, allowing very accurate and repeatable control of the scaffold geometry (and, thus, porosity) while allowing for the potential assembly of tissue-like spatial complexity. A wide range of applications of bioprinted acellular scaffolds have been reported, such as muscular tissues, liver tissues, cartilage, bone, skin, etc.² The specific material that composes the scaffold and any potential biological agents must be selected to recreate the nature of the engineered tissue. In this section, we focus on constructs with high mechanical strength, typically for engineered bone. The materials and AM processes for acellular scaffolds based on soft engineered tissues (e.g., skin, liver) are similar to the cell-laden ones and are, therefore, described in the section “Manufacturing Soft Materials for Cell Encapsulation” later in this article.

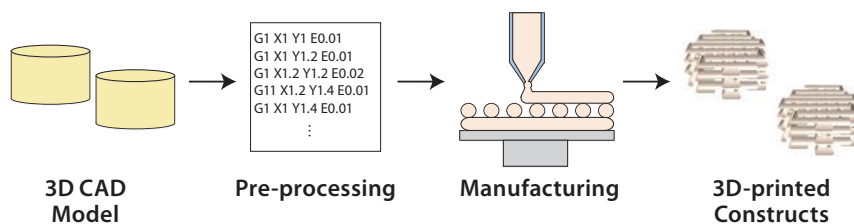


Figure 1. Overview of the 3D printing process.

Materials

Four categories of materials are highlighted based on their chemical nature. The first category is polymers,¹¹ such as collagen (Prod. Nos. C5483, C7624, H4417, etc.), fibrin (Prod. No. F5386), alginate, chitosan (Prod. Nos. 448869, 448877, 419419, etc.), poly(lactic acid) (PLA) (Prod. Nos. 764590, 765112, 764698, etc.), poly(glycolic acid) (PGA) (Prod. Nos. 457620 and 46746), polycaprolactone (PCL), and poly(propylene fumarate) (PPF). They can be highly bioresorbable and highly flexible in terms of chemical composition and processability. However, polymer-based scaffolds show a rapid decrease in stiffness over time once implanted. Calcium phosphate (CaPs) (Prod. No. 21218) based ceramic scaffolds, such as hydroxyapatite (HA) (Prod. Nos. 289396, 677418, 693863, etc.) and β -tricalcium phosphate (β -TCP) (Prod. Nos. 13204, 21218, and 49963)¹² have been extensively studied and used in clinical applications.¹³ CaPs scaffolds, being a major constituent of bones, exhibit high osteoconductivity. They also present high compressive strength, which can even be improved using dopant additives such as SiO_2 (Prod. Nos. 805890, 806587, 806765, etc.) or ZnO (Prod. Nos. 14439, 96479, etc.). But their processability is reduced and, therefore, possible geometries are limited. Metals are also used, usually titanium or stainless steel to ensure biocompatibility. They present a high mechanical strength but are non-biodegradable.¹³ Finally, composite materials have been developed by mixing two or more materials with the goal of combining the advantage of each individual material into one. One example is a polymer/ceramic composite, such as PCL/TCP or PCL/HA, in which the ceramic is integrated into the polymer to improve the mechanical integrity and bioactivity of the polymer.¹⁴ Composites show promising results for acellular scaffolds, with many potential combinations remaining to be explored.

Manufacturing Process

Numerous 3D printing and AM processes have been developed and commercialized since the 1980s,^{15,16} such as Stereolithography (SLA), Selective Laser Sintering (SLS), and Fused-deposition Modeling (FDM). These printing techniques can be used for the bioprinting of acellular scaffolds because they require less restrictive precautions like speed, temperature, toxicity and pressure for printing.

SLA consists of deflecting a laser beam in a horizontal plane to cure a photosensitive material in order to form a fixed layer.¹⁶ This layer is then moved along the vertical axis to allow the next adjoining layer to be created, as shown in **Figure 2**. This technology permits high resolution printing, with a layer thickness as small as 20 μm . In the horizontal plane, the resolution is defined by the diameter of the laser (around 250 μm); the use of Digital Light Projection (DLP) in place of a laser can improve the resolution to 70 μm . However, SLA limits the biochemical composition of the constructs to a single material, which must also be photosensitive.

SLS, in contrast, uses a high powered laser (**Figure 2**) to heat and fuse a powder-based material. By rastering the laser over the powder bed, the successive layers are fabricated. Once each layer is complete, another layer of powder is added to the top of the previous one, to be sintered

by the laser to form the next layer. This is repeated until the entire part is produced.¹⁶ Scaffolds manufactured using SLS show high mechanical strength and shape complexity, since sintering provides better bonds between each layer and the presence of unsintered powder gives support for each successive layer. The resolution and the surface finish can vary depending on the powder.

3D printing using FDM consists of the positioning of an extruding nozzle in order to deposit strands of material in 3D space. The extrusion material is thermally melted inside the nozzle, solidifying after cooling upon deposition to create a layer (**Figure 2**). Materials used for FDM must exhibit a molten phase, making certain polymers and composites well-suited for this process. Since the process is strand-based, it is highly suitable for porous structures. However, complex geometries, such as overhanging layers, are difficult to manufacture.

Manufacturing Soft Materials for Cell Encapsulation

Although acellular scaffolds can provide mechanical support and structural guidance for the growth of cells, post-processing cell seeding and/or biomolecule loading are required if cells and/or biomolecules need to be attached to the scaffold. This is a delicate task and does not allow for controlled attachment and spatial distribution of cells and biomolecules within the scaffold. However, loading is easier to achieve by encapsulating the cells and/or biomolecules directly in the printed material. By combining different cell types and growth factors according to designed biomimetic patterns, highly complex tissue constructs can be achieved.² Such tissue constructs have many applications, allowing significant progress toward 3D miniature tissue models for drug delivery tests. To meet the needs of these demanding applications, however, sterile conditions, non-toxic materials, mild fabrication processes, and relatively short processing time windows are required, impacting both the choice of the material and the printing process.

Materials

Cell encapsulation requires the printing material have high water content and sufficient porosity to enable cells to receive nutrients and oxygen from the environment as well as remove waste in order to stay alive. The material should be soft and biodegradable to allow the cells to spread, migrate, proliferate, and interact with each other.¹⁷ The most commonly used materials for cell encapsulation are hydrogels, which can be either natural or synthetic. Natural hydrogels, such as gelatin and collagen, are extracted from animal or human tissues, presenting intrinsic molecular interactions with cells. Synthetic hydrogels, such as poly(ethylene glycol) or PEG, are widely used in bioprinting because of the flexibility of their physical properties. Depending on the gelation principle, hydrogels can be divided into two categories: physical and chemical hydrogels.¹⁵ A hydrogel is formed "physically" by changing the temperature, pH value, or other physical properties, while a "chemical" hydrogel is produced by

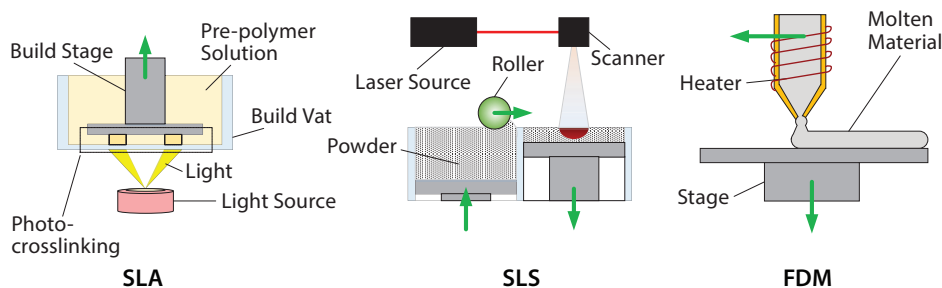


Figure 2. 3D printing processes for the manufacturing of acellular scaffolds.

crosslinking through covalent bonds. In the first case, the hydrogel can reverse back to its liquid state if the physical property is changed back to its initial state; whereas in the second case, the gelation is irreversible due to the water-insoluble network created by the covalent bonds formed. Chemical crosslinking is achieved by mixing two mutually reactive chemicals, while photocrosslinking is performed by exposing a solution composed of a photosensitive polymer and a photoinitiator to visible or UV light.¹⁶

Manufacturing Process

Inkjet-based bioprinting has been widely used to form 3D cell-laden constructs by continuously ejecting cell-laden droplets onto a destination stage using a thermal or an acoustic actuator. The nature of the print head designates the 3D construct be built dot by dot for each layer. Inkjet-based bioprinters are common for bioprinting applications because they have a fast printing speed, are compatible with biological components, and are low cost. The viscosity of the printing material should be considered when choosing this printing method in order to reduce clogging the print head.

SLA can also be used to manufacture cell-laden constructs by adding cells to an uncrosslinked pre-polymer material. Visible light is the preferred light source for crosslinking when using DLP due to cell sensitivity to UV exposure and changes in temperature. While SLA offers high resolution, the tradeoff between printing quality and total processing time should be considered to yield optimal conditions for cell viability. SLA requires a larger amount of material than other bioprinting methods due to the requirement of filling the vat (**Figure 3**) with the printing material, which presents a major drawback if using expensive materials.

Another way to print hydrogel constructs is extrusion. To do this, a chamber is filled with cell-laden biomaterial, then using either pneumatic or piston-driven extrusion, the material is propelled through the print head. In order to create cell-laden constructs layer by layer, the print head robotically follows the desired path. For a physically formed hydrogel, the struts are extruded and gelled on stage upon change in pH, temperature, or other physical condition. Photocrosslinkable materials can also be used for this process. Once a layer of pre-polymer solution is extruded, it is crosslinked by exposure to light. Although the printing speed and the amount of extrusion can be precisely controlled, significant shear stress on the material can impact cell viability and should be carefully avoided.

Laser-based bioprinting is a commonly used technique in which a laser is used to transfer cell-laden materials from a source plate to the deposition stage. To achieve this transfer, the source plate is coated in a double layer with a laser-absorbing layer and a donor layer of biomaterial (**Figure 3**). When the laser pulse focuses on the laser-absorbing layer, the heated region generates a bubble to propel and deposit a droplet of biomaterial onto the destination stage. Use of a laser instead of a nozzle allows for the deposition of highly viscous materials with high accuracy. However, the heat generated by the laser hinders cell viability, and this process is the most limited in terms of vertical constructs.

Current Challenges and Perspectives

We have provided a brief overview of the current state of the art in bioprinting based on the two predominant approaches. In the first approach, acellular scaffolds are used to provide high resolution and highly reproducible implantable templates to promote cell function and tissue regeneration. In the second approach, cells are encapsulated directly in the material for integration inside a construct during printing. Materials used for this method contain a high ratio of water and are, thus, considered to be soft materials in terms of stiffness. While the first approach has been deliberately dedicated to stiffer materials in this section, it should be noted that acellular scaffolds based on soft materials can also be achieved using processes described in the earlier section "Manufacturing Soft Materials for Cell Encapsulation."

While already showing very promising results, bioprinting is still in its early stage, and several challenges remain to be addressed to move the field forward. For example, as previously discussed, current 3D bioprinting approaches have limited capability for integrating the soft and rigid multifunctional components required for tissues and organs because of their inherent heterogeneity in mechanical, physical, chemical, and biological properties and functions. As a step toward this goal, our lab has developed a 3D hybrid bioprinter (Hybprinter) that can continuously and rapidly integrate cell-laden soft materials and rigid frame materials using FDM, SLA, and extrusion-based techniques in a controllable and automated manner under a single platform.¹⁸ By taking advantage of each process, we are able to manufacture constructs with both acellular scaffolds and cell-laden hydrogels, a step toward highly complex multi-material constructs.

While bioprinting shows promise in tissue engineering, improvements in the printing processes are required. Increased speed should be considered in order to ease scale-up for acellular scaffolds and improve cell viability for cell-laden constructs. Moreover, higher resolution is required, in particular for the manufacturing of heterogeneous composite tissues and vascularized tissues. Vascularization is one of the key components and arguably the greatest challenge of tissue engineering.¹⁹ Such tissues consist of a highly complex vascular network, from millimeter-sized vessels to micrometer-scale capillaries. Reproducing such a network is a huge challenge, and up to now it has mainly been addressed by providing sufficient space in the porous scaffold for vascular tissues to spontaneously develop. A 3D printing process such as two-photon polymerization²⁰ allows the manufacturing of parts with a micron-to-millimeter range of size and is, therefore, considered as a promising bioprinting process for the manufacturing of vascularized tissue constructs.

Research should also focus on the development of new materials that have improved biological properties and are suitable for bioprinting. Additionally, research should focus on using the current or future technologies to improve assembly of existing biomaterials to better mimic the complexity of the ECM, or the combination of both. Available materials for cell-laden tissue constructs dedicated to bioprinting are

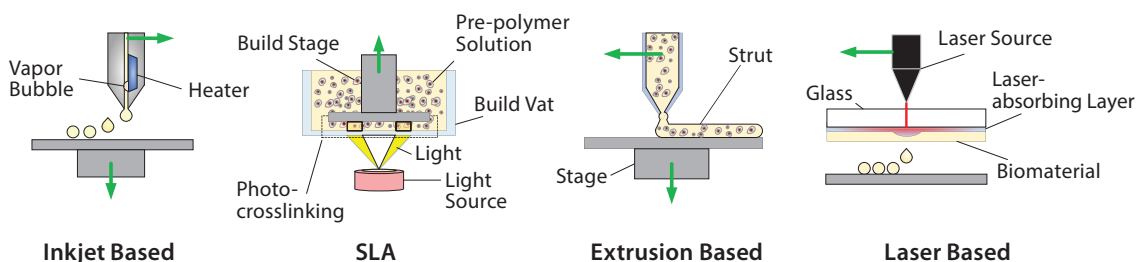


Figure 3. 3D printing process for the manufacturing of soft materials for cell encapsulation.

currently limited, but improved imaging capability and a fundamental understanding of the complexity of tissues and developmental biology will contribute to the development of new materials and bioprinting technologies. It remains to be seen to what extent biomimetic complexity of the bioprinted constructs either in chemistry or in physical structure is necessary to achieve better healing and restoration of lost functions.

A growing number of AM applications are emerging, with bioprinting emerging as one of the most promising and challenging manufacturing processes due to the potential impact on global healthcare concerns like aging, organ transplantation, cancer therapy, and personalized and precision medicine. In the future, bioprinting has the potential to become both a source of miniature disease and toxicology models for the pharmaceutical industry and as a source of life-sized tissue/organ replacements for clinical treatments.

Acknowledgments

We would like to acknowledge the financial support of the following agencies: NIH R01AR057837 (NIAMS), NIH R01DE021468 (NIIDCR), DOD W911NF-14-1-0545 (DURIP), DOD W81XWH-10-1-0966 (PRORP), and Stanford Coulter Translational Seed Grant.

References

- (1) Stock, U. A.; Vacanti, J. P. *Annu. Rev. Med.* **2001**, *52*, 443–51. doi: 10.1146/annurev.med.52.1.443. PubMed PMID: WOS:000167302900025.
- (2) Langer, R.; Vacanti, J. P. *Science*. **1993**, *260*(5110), 920–6. Epub 1993/05/14. PubMed PMID: 8493529.
- (3) Griffith, L. G.; Naughton, G. *Science*. **2002**, *295*(5557), 1009+. doi: 10.1126/science.1069210. PubMed PMID: WOS:000173793000043.
- (4) Dababneh, A. B.; Ozbolat, I. T. *J. Manuf. Sci. E-T ASME*. **2014**, *136*(6), 11. doi: 10.1115/1.4028512. PubMed PMID: WOS:000344393000018.
- (5) Smith, I. O.; Liu, X. H.; Smith, L. A.; Ma, P. X. *WIREs Nanomed. Nanobiotechnol.* **2009**, *1*(2), 226–36. doi: 10.1002/wnan.026. PubMed PMID: WOS:000276839400008.
- (6) Mironov, V.; Reis, N.; Derby, B. *Tissue Engineering* **2006**, *12*(4), 631–4. doi: 10.1089/ten.2006.12.631. PubMed PMID: WOS:000237494400001.
- (7) Sears, N. A.; Seshadri, D. R.; Dhavalikar, P. S.; Cosgriff-Hernandez, E. *Tissue Eng. Part B, Rev.* **2016**. Epub 2016/02/10. doi: 10.1089/ten.TEB.2015.0464. PubMed PMID: 26857350.
- (8) Bose, S.; Vahabzadeh, S.; Bandyopadhyay, A. *Mater. Today* **2013**, *16*(12), 496–504. doi: 10.1016/j.mattod.2013.11.017. PubMed PMID: WOS:000328640100018.
- (9) Hutmacher, D. W. *Biomaterials* **2000**, *21*(24), 2529–43. doi: 10.1016/s0142-9612(00)00121-6. PubMed PMID: WOS:000089861700006.
- (10) Bose, S.; Roy, M.; Bandyopadhyay, A. *Trends Biotechnol.* **2012**, *30*(10), 546–54. doi: 10.1016/j.tibtech.2012.07.005. PubMed PMID: WOS:000309946600007.
- (11) Liu, X. H.; Ma, P. X. *Ann. Biomed. Eng.* **2004**, *32*(3), 477–86. doi: 10.1023/B:ABME.0000017544.36001.8e. PubMed PMID: WOS:000222465100019.
- (12) Sweet, L.; Kang, Y.; Czisch, C.; Wittek, L.; Shi, Y.; Smay, J.; et al. *Plos One*. **2015**, *10*(10). doi: 10.1371/journal.pone.0139820. PubMed PMID: WOS:000362510600085.
- (13) Lichte, P.; Pape, H. C.; Pufe, T.; Kobbe, P.; Fischer, H. *Injury* **2011**, *42*(6), 569–73. Epub 2011/04/15. doi: 10.1016/j.injury.2011.03.033. PubMed PMID: 21489531.
- (14) Lu, L.; Zhang, Q.; Wootton, D.; Chiou, R.; Li, D.; Lu, B.; Lelkes, P.; Zhou, J. Biocompatibility and biodegradation studies of PCL/beta-TCP bone tissue scaffold fabricated by structural porogen method. *Journal of Materials Science-Materials in Medicine* **2012**, *23* (9), 2217–2226.
- (15) Hoffman, A. S. *Adv. Drug Deliv. Rev.* **2002**, *54*(1), 3–12. doi: http://dx.doi.org/10.1016/S0169-409X(01)00239-3.
- (16) Elomaa, L.; Pan, C. C.; Shanjan, Y.; Malkovskiy, A.; Seppala, J. V.; Yang, Y. *J. Mater. Chem. B*. **2015**, *3*(42):8348–58. doi: 10.1039/c5tb01468a.
- (17) Elomaa, L.; Kang, Y.; Seppälä, J. V.; Yang, Y. *J. Polym. Sci. A Polym. Chem.* **2014**, *52*(23), 3307–15. doi: 10.1002/pola.27400.
- (18) Shanjan, Y.; Pan, C. C.; Elomaa, L.; Yang, Y. *Biofabrication* **2015**, *7*(4), 045008. Epub 2015/12/20. doi: 10.1088/1758-5090/7/4/045008. PubMed PMID: 26685102.
- (19) Mercado-Pagan, A. E.; Stahl, A. M.; Shanjan, Y.; Yang, Y. *Ann. Biomed. Eng.* **2015**, *43*(3), 718–29. Epub 2015/01/27. doi: 10.1007/s10439-015-1253-3. PubMed PMID: 25616591.
- (20) Weiß, T.; Berg, A.; Fiedler, S.; Hildebrand, G.; Schade, R.; Schnabelrauch, M.; et al. Two-Photon Polymerization for Microfabrication of Three-Dimensional Scaffolds for Tissue Engineering Application. In: Dössel O, Schlegel WC, editors. *World Congress on Medical Physics and Biomedical Engineering, September 7–12, 2009, Munich, Germany: Vol 25/10 Biomaterials, Cellular and Tissue Engineering, Artificial Organs*. Berlin, Heidelberg: Springer Berlin Heidelberg; **2010**. p. 140–2.

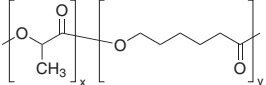
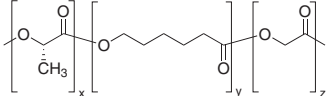
Biodegradable Polymers

For more information on these products, visit aldrich.com/biopoly.

Polycaprolactones

Name	Structure	Molecular Weight	Transition Temperature	Prod. No.
Polycaprolactone		average M_n ~10,000	T_g -60 °C	440752-5G 440752-250G 440752-500G
		average M_n 45,000	-	704105-100G 704105-500G
		average M_n 80,000	-	440744-5G 440744-250G 440744-500G
Polycaprolactone dimethacrylate		average M_n 550	-	802115-2G
		average M_n 2,250	-	802158-2G
Polycaprolactone diol		average M_n ~530	softening point 35 °C	189405-250G 189405-500G
		average M_n ~2,000	softening point 50 °C	189421-250G 189421-500G
Polycaprolactone trimethacrylate		average M_n 950	-	799556-2G
Polycaprolactone triol		average M_n ~300	softening point 10 °C	200387-250G 200387-500G
		average M_n ~900	softening point 30 °C	200409-250G 200409-500G

Block PCL Polymers

Name	Structure	Composition	Inherent Viscosity	Transition Temperature	Prod. No.
Poly(D,L-lactide-co-caprolactone)		D,L-lactide 86 mol %	0.7-0.9 dL/g in chloroform	T _g 16 °C	457647-5G
		D,L-lactide 40 mol %	0.7-0.9 dL/g in chloroform	T _m 31 °C, DSC, onset	457639-5G
Poly(L-lactide-co-caprolactone-co-glycolide)		glycolide 10% L-lactide 70% caprolactone 20%	-	-	568562-1G 568562-5G

Poly(lactide-co-glycolide) Copolymers

Name	Feed Ratio	End Group	Molecular Weight	Degradation Time (months)	Prod. No.
Resomer® RG 502 H, Poly(D,L-lactide-co-glycolide)	lactide:glycolide 50:50	acid terminated	M _w 7,000-17,000	<3	719897-1G 719897-5G
Resomer® RG 503 H, Poly(D,L-lactide-co-glycolide)		acid terminated	M _w 24,000-38,000	<3	719870-1G 719870-5G
Resomer® RG 504 H, Poly(D,L-lactide-co-glycolide)		acid terminated	M _w 38,000-54,000	<3	719900-1G 719900-5G
Resomer® RG 502, Poly(D,L-lactide-co-glycolide)		ester terminated	M _w 7,000-17,000	<3	719889-1G 719889-5G
Resomer® RG 503, Poly(D,L-lactide-co-glycolide)		ester terminated	M _w 24,000-38,000	<3	739952-1G 739952-5G
Resomer® RG 504, Poly(D,L-lactide-co-glycolide)		ester terminated	M _w 38,000-54,000	<3	739944-1G 739944-5G
Resomer® RG 505, Poly(D,L-lactide-co-glycolide)		ester terminated	M _w 54,000-69,000	<3	739960-1G 739960-5G
Resomer® RG 653 H, Poly(D,L-lactide-co-glycolide)	lactide:glycolide 65:35	acid terminated	M _w 24,000-38,000	<5	719862-1G 719862-5G
Resomer® RG 752 H, Poly(D,L-lactide-co-glycolide)	lactide:glycolide 75:25	acid terminated	M _w 4,000-15,000	<6	719919-1G 719919-5G
Resomer® RG 756 S, Poly(D,L-lactide-co-glycolide)		ester terminated	M _w 76,000-115,000	<6	719927-1G 719927-5G
Poly(D,L-lactide-co-glycolide)	lactide:glycolide 85:15	ester terminated	M _w 50,000-75,000	<6	430471-1G 430471-5G
Resomer® RG 858 S, Poly(D,L-lactide-co-glycolide)		ester terminated	M _w 190,000-240,000	<9	739979-1G 739979-5G

Well-defined Poly(L-lactide)s

Name	Molecular Weight (M _n)	PDI	Degradation Time (years)	Prod. No.
Poly(L-lactide)	5,000	≤1.2	>3	764590-5G
	10,000	≤1.1	>3	765112-5G
	20,000	≤1.1	>3	764698-5G

Well-defined Poly(D,L-lactide)s

Name	Molecular Weight (M _n)	PDI	Degradation Time (months)	Prod. No.
Poly(D,L-lactide)	5,000	≤1.1	<6	764612-5G
	10,000	≤1.1	<6	764620-5G
	20,000	≤1.3	<6	767344-5G

Poly(L-lactide)s



Name	End Group	Molecular Weight	Degradation Time (years)	Prod. No.
Resomer® L 206 S, Poly(L-lactide), ester terminated	ester terminated	-	>3	719854-5G 719854-25G
Poly(L-lactide)	ester terminated	average M_n 50,000	>3	94829-1G-F 94829-5G-F
	ester terminated	M_n 59,000 M_w 101,000	>3	93578-5G-F
	ester terminated	M_w ~260,000	>3	81273-10G
	ester terminated	M_n 103,000 M_w 259,000	>3	95468-1G-F 95468-5G-F

Poly(D,L-lactide)s



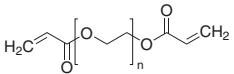
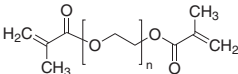
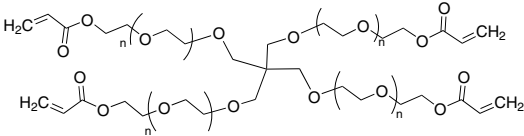
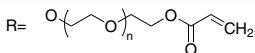
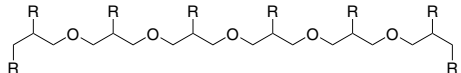
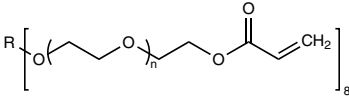
Name	End Group	Molecular Weight	Degradation Time (months)	Prod. No.
Resomer® R 202 H, Poly(D,L-lactide)	acid terminated	M_w 10,000-18,000	<6	719978-1G 719978-5G
Resomer® R 203 H, Poly(D,L-lactide)	acid terminated	M_w 18,000-24,000	<6	719943-1G 719943-5G
Resomer® R 202 S, Poly(D,L-lactide)	ester terminated	M_w 10,000-18,000	<6	719951-1G 719951-5G
Resomer® R 203 S, Poly(D,L-lactide)	ester terminated	M_w 18,000-28,000	<6	719935-1G 719935-5G

End-functionalized Low PDI Poly(L-lactide)

Name	Structure	Molecular Weight	PDI	Prod. No.
Poly(L-lactide), acrylate terminated		average M_n 2,500	≤ 1.2	775991-1G
		average M_n 5,500	≤ 1.2	775983-1G
Poly(L-lactide), amine terminated		average M_n 2,500	≤ 1.3	776378-1G 776378-5G
		average M_n 4,000	≤ 1.2	776386-1G 776386-5G
		average M_n 5,000	<1.2	774146-1G
Poly(L-lactide), N-2-hydroxyethylmaleimide terminated		average M_n 2,000	≤ 1.2	746797-1G 746797-5G
		average M_n 5,000	<1.2	746517-1G 746517-5G
Poly(L-lactide), 2-hydroxyethyl, methacrylate terminated		average M_n 2,000	≤ 1.1	771473-1G 771473-5G
		average M_n 5,500	≤ 1.2	766577-1G 766577-5G
Poly(L-lactide), propargyl terminated		average M_n 2,000	≤ 1.1	774162-1G
		average M_n 5,000	≤ 1.1	774154-1G
Poly(L-lactide), thiol terminated		average M_n 2,500	≤ 1.2	747386-1G 747386-5G
		average M_n 5,000	≤ 1.2	747394-1G 747394-5G

Poly(ethylene glycol)s (PEG)

For a complete list of available materials, visit aldrich.com/peg.

Structure	Name	Molecular Weight	Prod. No.
	Poly(ethylene glycol) diacrylate	average M_n 2,000	701971-1G
	Acrylate-PEG3500-Acrylate	average M_n 3,500	JKA4048-1G
	Poly(ethylene glycol) diacrylate	average M_n 6,000	701963-1G
	Poly(ethylene glycol) diacrylate	average M_n 10,000	729094-1G
	Poly(ethylene glycol) diacrylate	PEG average M_n 20,000 (n~450) average M_n 20,000	767549-1G
	Poly(ethylene glycol) dimethacrylate	average M_n 2000	687529-1G
	Poly(ethylene glycol) dimethacrylate	average M_n 6,000	687537-1G
	Poly(ethylene glycol) dimethacrylate	average M_n 10,000	725684-1G
	4arm-PEG10K-Acrylate	average M_n 10,000	JKA7068-1G
	4arm-PEG20K-Acrylate	average M_n 20,000	JKA7034-1G
	8arm-PEG20K-Acrylate, hexaglycerol core	average M_n 20,000	JKA8005-1G
	8arm-PEG10K-Acrylate, tripentaerythritol core	average M_n 10,000	JKA10021-1G
	8arm-PEG10K-Acrylate, tripentaerythritol core	average M_n 10,000	JKA10021-1G

R = tripentaerythritol core structure

3D AND 4D PRINTING TECHNOLOGIES: AN OVERVIEW



Wonjin Jo,* Kyung Sung Chu, Heon Ju Lee, Myoung-Woon Moon
3D Printing Group, Computational Science Research Center
Korea Institute of Science and Technology, 02792, Seoul, Republic of Korea
*Email: wjjo@kist.re.kr

Introduction

Three-dimensional (3D) printing technology, also called additive manufacturing (AM), has recently come into the spotlight because of its potential high-impact implementation in applications ranging from personal tools to aerospace equipment. Even though 3D printing technology has only recently emerged as a hot topic, its history can be traced back to 1983 when the first 3D printer was created by Charles W. Hull, co-founder of 3D Systems. Since then, new and wide-ranging applications and markets for 3D printers have appeared rapidly, especially with the expiration of a number of core 3D printing patents owned by Stratasys Inc. and 3D Systems Inc. Users can easily build or modify 3D printers by themselves or take advantage of the rapidly growing availability of inexpensive 3D printers. The recent availability of highly capable 3D design software and 3D design websites (e.g., Shapeway and Thingiverse) allows the sharing of user-created free 3D digital design files or models, leading to more access to 3D printers and additional proliferation of 3D printing technology. When compared to traditional manufacturing technologies such as casting, machining, and drilling, 3D printing is considered an efficient technology in the areas of energy and materials, utilizing up to 90% of materials and providing up to 50% energy savings.¹

As 3D printing becomes more than just a simple production process, it has come to support a convergence of technologies and applications such as sports equipment, food packaging, and jewelry, as well as products in the high tech fields of aerospace, medicine, architecture, education,^{2,3} automotive industry, military support, and others. At the 2016 New York Fashion Week, two unique 3D printed dresses were unveiled. These masterpieces were produced through a collaboration between fashion designers and the 3D printing company, Stratasys.⁴ The complex designs (e.g., mixing a variety of interlocking weaves, biomimicking natural animal textures) and cutting-edge material (e.g., nano-enhanced elastomeric 3D printing material) gave the dresses durability and flexibility. The area of regenerative medicine has also achieved impressive applications within the 3D printing field. Dr. Anthony Atala's team from the Wake Forest Institute for Regenerative Medicine has successfully used 3D printing technology to fabricate living organs and tissue (including muscle structures, and bone and ear tissue).^{5,6} These bioprinted body parts are capable of generating functional replacement tissue.⁷ NASA

has also been implementing 3D printing techniques and 3D printers to develop materials that allow astronauts to repair or replace essential parts and build structures in space. NASA recently collaborated with researchers at Washington State University to fabricate a replica of a moon rock using raw lunar regolith simulant and 3D laser printing technology.^{8,9} The assembly of modular construction materials using giant 3D printers for use in the housing industry has gained significant interest, especially for poorer countries, during natural disasters, or sudden emergencies. Some 3D companies have succeeded in building houses or bridges with cement, sand, or concrete materials.¹⁰⁻¹²

The rapidly decreasing cost, improved software design, and increasing range of printable materials have helped to bring about a new technology called four-dimensional (4D) printing. 4D printing provides printed objects with the ability to change form or function with time according to various stimuli such as heat, water, current, or light (Figure 1A).¹³ The essential difference between 4D printing and 3D printing is the addition of smart design, or responsive materials that cause time-dependent deformations of objects. This review covers both 3D and 4D printing processes and shows the materials related to different printing types.

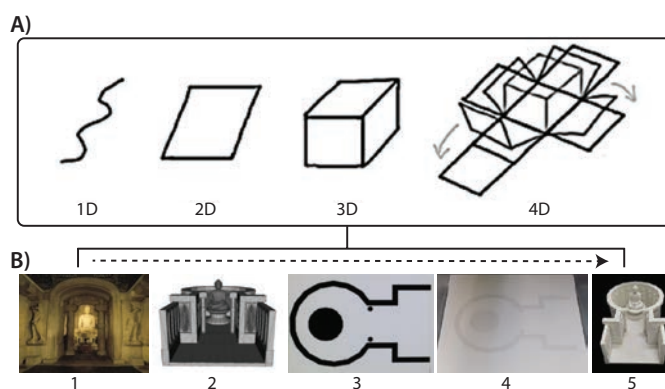


Figure 1. A) Schematic of 1-, 2-, 3-, and 4D concepts. B) The process of 3D and 4D printing technology involves three general stages: (1–2) modeling; (3–4) printing; and (5) finishing.

The Process of 3D and 4D Printing Technology

3D printing is the process of fabricating objects by building up materials layer by layer. Figure 1B shows the 3D printing process from modeling to final printing. Based on the use of computer-aided design (CAD) describing the geometry and the size of the objects to be printed, a complicated 3D model is created in a printable standard tessellation language (STL) file format (Figure 1B1,1B2). Then, it is sliced into a series of digital cross-sectional layers in accordance with the layer

thickness setting (Figure 1B3). Upon completion of the model, the object is fabricated by a 3D printer through the layer-by-layer fabrication process based on a series of 2D layers to create a static 3D object (Figure 1B4,1B5). 3D printing can involve different types of materials such as thermoplastic polymer, powder, metal, UV curable resin, etc.

Four-dimensional printing incorporates a time component to the 3D printed objects, making the design process more important. 4D-printed structures must be preprogrammed in detail based on the transforming mechanism of controllable smart materials that incorporate time-dependent material deformations.¹³ Figure 2A–C show 3D structures that self-fold based on the thermal activation of spatially variable patterns printed with a variety of shape memory polymers. Each polymer has a different thermal-dependent behavior that can make the box self-fold in a time-sequential manner based on smart design and thermomechanical mechanisms.¹⁴ The choice of materials for 4D printing is significant, however, because most 3D printing materials are designed only to produce rigid, static objects. Recently, some smart shape alloy/polymer memory materials have been developed to utilize their self-assembled behaviors driven by heat, UV, or water absorption-driven as shown in Figure 2D–F.¹⁵ For example, the temperature-responsive artificial hand shown in Figure 2F was printed with a temperature-responsive TPU (thermal polyurethane) filament. It has the ability to contract or expand in response to specific temperatures. In addition, multi-materials having different environmental behaviors are also useful in 4D printing. A research group at the Massachusetts Institute of Technology used two different materials with different porosities and water-absorption abilities to print transformable structures.^{16,17} It was composed of a porous water-absorbing material on one side and a rigid waterproof material on the opposite side. When exposed to water, the water-absorbing side increased in volume while the other side remained unchanged, resulting in shape deformation.

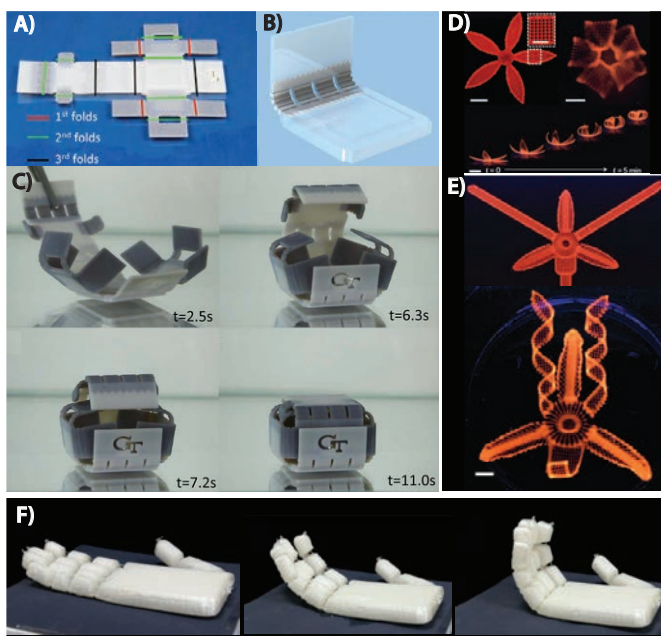


Figure 2. A–B) The design of the folding box with different materials assigned at different hinges. C) Upon heating, the programmed 3D printed sheet folds into a box with a self-locking mechanism. Copyright 2015, rights managed by Nature Publishing Group. D–E) The resulting swollen flower structures were generated by biomimetic 4D printing with composite hydrogel and cellulose fibrils. Copyright 2016, rights managed by Nature Publishing Group. F) The temperature-responsive artificial hand was made with temperature-responsive TPU filament.

Classification of 3D and 4D Printing Technologies

The 3D and 4D printing technologies are classified into different printing processes, defined mainly by the types of materials used. The selection of materials has a direct influence on the mechanical or thermal properties, as well as the transformation stimuli of the finished objects. This section describes the three most common types of 3D and 4D printing and reviews the most frequently used materials for these processes.

Fused-deposition Modeling (FDM)

The FDM method operates by extruding thermoplastic materials and placing the semi-molten materials onto a stage to fabricate a 3D structure layer by layer.¹⁸ More specifically, the thermoplastic filament is first led to an extruder which feeds and retracts the filament in precise amounts. The filament is melted by a heater block set to the melting temperature and moved through the extrusion nozzle tip by two rollers. The extruded filament is deposited as the print head traces the design of each defined cross-sectional layer of the desired structure by a digitally positioned mechanism. Then, the stage moves to the Z position in accordance with the setting value of layer thickness. These steps are repeated to complete fabrication of the 3D structure.

One advantage of FDM is the availability of a variety of filament materials as shown in Figure 3. A wide selection of FDM filaments are commercially available with different strength and temperature properties, such as ABS (acrylonitrile butadiene styrene, Prod. Nos. 3DXABS001–3DXABS0016), nylon (Prod. Nos. 3DXION001–3DXION004), PET (polyethylene terephthalate, Prod. Nos. 900095 and 900125), TPU (thermal polyurethane, Prod. Nos. 900126 and 900128), POM (polyoxymethylene), PC (polycarbonate), HIPS (high impact polystyrene), and PVA (polyvinyl alcohol), among others. In addition, some materials can be used as a raw material for mixing with other functional materials to improve specific functions. Among them, the PLA (polylactic acid) filament is a popular choice due to the many available properties as shown in Figure 3. Due to the thermoplastic behavior, many FDM filaments can also be used as 4D materials under applied heat change.

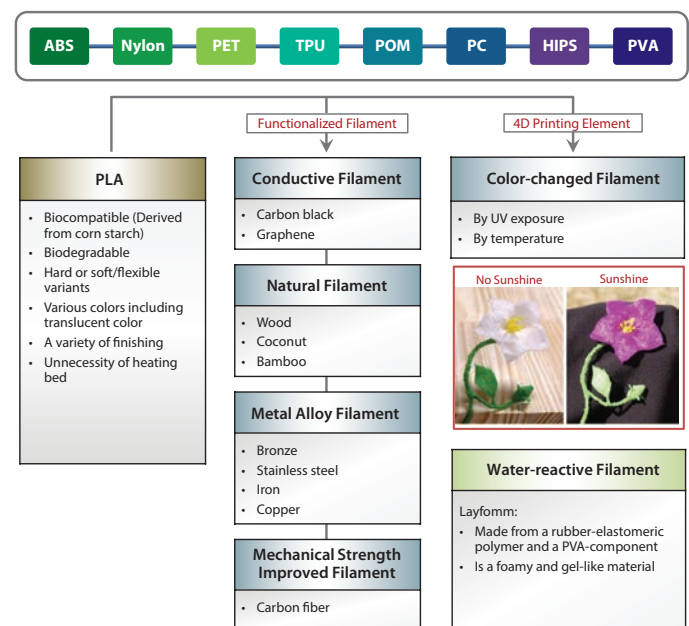


Figure 3. Thermoplastic filaments for Fused-deposition Modeling (FDM). The FDM-printed flower was made with a color changed filament under UV exposure.

Powder Bed and Inkjet Head 3D Printing (PBP)

The PBP process is an adaptation of inkjet printing. In this process, a layer of powder is first deposited and rolled to ensure uniform thickness, then the inkjet print head drops binder in a specified pattern as it moves, to form a single layer of a printed object across the bed of powder. The next powder layer is distributed over the deposited liquid binder, and this process is repeated, with each layer adhering to the last. Support structures are not required in PBP due to the ease of removing unbound powder using an air gun, after solidification of the finished object. The use of multiple print heads with colored binder, allows printing in full color.

Among the variety of powders available, calcium sulfate (CaSO_4 , Prod. Nos. 255696 and 237132) is one of the most widely-used because of its ability to react with water-based binders. It can react with water-based solutions rapidly and change into gypsum ($\text{CaSO}_4 \cdot 2\text{H}_2\text{O}$) in a solid state.¹⁹ In this method, the binding strength is the key factor in determining the physical and chemical properties of the printed device. Therefore, the proper combination of powder and binder should be carefully considered.

Very recently, Voxeljet developed the world's largest industrial PBP system (VX4000) for sand molds. The largest cohesive build space is $4,000 \times 2,000 \times 1,000$ mm (L \times W \times H) with 300 μm of a layer applied in one cycle.²⁰

Stereolithography (SLA)

SLA combines ultraviolet (UV) or visible laser light with curable liquid photopolymer resins. To create each layer, a laser beam illuminates a 2D cross-section of the object in a vat of resin, allowing the resin to solidify. Next, the object is raised by an equal distance of layer thickness to fill resin under and maintain contact with the bottom of the object. This process is repeated until the entire model is completed, at which point the platform is raised out of the vat and the excess resin is drained. Finally, the SLA object is finished by washing and curing under UV light. SLA produces a smoother surface on the final product compared to other 3D printing methods, as a result of using liquid photopolymers. Although SLA can produce a wide variety of shapes, its drawbacks include a significant amount of resin waste and the need for extensive cleaning after fabrication. Furthermore, resins used in the process are limited to either epoxy or acrylic bases, most of which can shrink upon polymerization.

A recent advance in SLA significantly decreases printing time. Carbon 3D Inc. announced a new continuous liquid interface production (CLIP) method that can print an object 100 times faster than existing methods by creating an oxygen depletion zone (dead zone) in liquid resins as shown in Figure 4.²¹ The introduction of a unique oxygen-permeable window in the resin reservoir creates a thin liquid interface of uncured resin between the window and printing part. This oxygen-depleted dead zone allows for continuous translation and curing of the resin above the dead zone to form a consistent solid part.

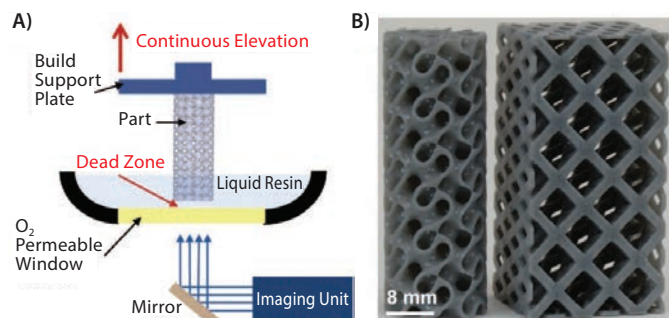


Figure 4. A) Schematic of a CLIP printer. B) The resulting parts via CLIP at print speeds of 500 mm/hour. Copyright 2015, The American Association for the Advancement of Science.

Future Prospects

Three-dimensional printing technology is highly versatile and efficient with respect to design, fabrication, and applications. 4D printing may be of great importance in the future due to its potential to redefine manufacturing-related industries. However, the technology must be further refined before it can replace conventional manufacturing methods. Therefore, future research and investment in 3D and 4D printing technologies are imperative to bring about improvements in essential areas including materials, printer systems, and product markets.

References

- (1) Pangaea Blog, posted by Matthew Cohen on May 2013. <http://www.pangaeaventures.com/blog/additive-manufacturing-printing-a-better-and-cleaner-world>
- (2) Science News section of ScienceDaily, posted on July 2014. <http://www.sciencedaily.com/releases/2014/07/140702102601.htm>
- (3) Jo, W.; I, J. H.; Harianto, R. A.; So, J. H.; Lee, H.; Lee, H. J.; Moon, M.-W. *J. Vis. Impair. Blind.* **2016**, *110*, in press.
- (4) 3Ders.org, posted by Tess on Feb 2016. <http://www.3ders.org/articles/20160216-threearfour-unveils-two-spectacular-3d-printed-dresses-at-new-york-fashion-week.html>
- (5) Kang, H. W.; Lee, S. J.; Ko, I. K.; Kengla, C.; Yoo, J. J.; Atala, A. *Nat. Biotechnol.* **2016**, *34*(3), 312–319.
- (6) Shafiee, A.; Atala, A. *Trends Mol. Med.* **2016**, *22*(3), 254–265.
- (7) The Guardian, posted by Tim Radford on Feb 2016. <https://www.theguardian.com/science/2016/feb/15/bioprinter-creates-bespoke-lab-grown-body-parts-for-transplant>
- (8) SPACE.com, posted by Megan Gannon on Jan 2012. <http://www.space.com/18694-moon-dirt-3d-printing-lunar-base.html>
- (9) Balla, V. K.; Roberson, L. B.; O'connor, G. W.; Trigwell, S.; Bose, S.; Bandyopadhyay, A. *Rapid Prototype J.* **2012**, *18*, 451–257.
- (10) WASP, posted on Mar 2015. <http://www.wasproject.it/w/en/new-extruder-wasp-can-truly-realize-house-dream/>
- (11) 3DPrint.com, posted by Eddie Krassenstein on Aug 2014. <http://3dprint.com/12933/3d-printed-castle-complete/>
- (12) 3Ders.org, posted by Kira on Jan 2015. <http://www.3ders.org/articles/20150118-winsun-builds-world-first-3d-printed-villa-and-tallest-3d-printed-building-in-china.html>
- (13) Choi, J.; Kwon, O. C.; Jo, W.; Lee, H. J.; Moon, M.-W. *3D Printing and Additive Manufacturing* **2015**, *2*, 159–167.
- (14) Mao, Y.; Yu, K.; Isakov, M. S.; Wu, J.; Dunn, M. L.; Jerry Qi, H. *Sci. Rep.* **2015**, *5*, 13616.
- (15) Sydney Gladman, A.; Matsumoto, E. A.; Nuzzo, R. G.; Mahadevan, L.; Lewis, J. A. *Nat. Mater.* **2016**, advance online publication.
- (16) Tibbits, S. *Archit. Des.* **2014**, *84*, 116–121.
- (17) Raviv, D.; Zhao, W.; McKnelly, C.; Papadopoulou, A.; Kadambi, A.; Shi, B.; Hirsch, S.; Dikovskiy, D.; Zyracki, M.; Olguin, C.; Raskar, R.; Tibbits, S. *Sci. Rep.* **2014**, *4*, 7422.
- (18) Jo, W.; Kim, D. H.; Lee, J. S.; Lee, H. J.; Moon, M.-W. *RSC Adv.* **2014**, *4*, 31764–31770
- (19) Liu, W.; Wu, C.; Liu, W.; Zhai, W.; Chang, J. J. *Biomed. Mater. Res. B Appl. Biomater.* **2013**, *101B*, 279–286.
- (20) <http://www.voxeljet.de/en/systems/vx4000/>
- (21) Tumbleston, J. R.; Shirvanyants, D.; Ermoshkin, N.; Janusziewicz, R.; Johnson, A. R.; Kelly, D. et al. *Science* **2015**, *347*, 1349–1352.

3D Printing Filaments

For a complete list of available materials, visit aldrich.com/3dp.

ABS

Weight = 2.2 lb spool

Color	Diameter (mm)	Prod. No.
black	1.75	3DXABS001-1EA
	2.85	3DXABS002-1EA
blue	1.75	3DXABS003-1EA
	2.85	3DXABS004-1EA
green	1.75	3DXABS005-1EA
	2.85	3DXABS006-1EA
natural	1.75	3DXABS007-1EA
	2.85	3DXABS008-1EA
orange	1.75	3DXABS009-1EA
	2.85	3DXABS010-1EA
red	1.75	3DXABS011-1EA
	2.85	3DXABS012-1EA
white	1.75	3DXABS013-1EA
	2.85	3DXABS014-1EA
yellow	1.75	3DXABS015-1EA
	2.85	3DXABS016-1EA

PLA

Weight = 2.2 lb spool

Color	Diameter (mm)	Prod. No.
black	1.75	3DXPLA001-1EA
	2.85	3DXPLA002-1EA
blue	1.75	3DXPLA003-1EA
	2.85	3DXPLA004-1EA
green	1.75	3DXPLA005-1EA
	2.85	3DXPLA006-1EA
natural	1.75	3DXPLA007-1EA
	2.85	3DXPLA008-1EA
orange	1.75	3DXPLA009-1EA
	2.85	3DXPLA010-1EA
red	1.75	3DXPLA011-1EA
	2.85	3DXPLA012-1EA
white	1.75	3DXPLA013-1EA
	2.85	3DXPLA014-1EA
yellow	1.75	3DXPLA015-1EA
	2.85	3DXPLA016-1EA

Carbon Fiber Reinforced Filaments

Weight = 1.65 lb spool

Description	Diameter (mm)	Prod. No.
3DXMAX™ CFR-PLA carbon fiber reinforced PLA 3D printing filament	1.75	3DXCFR002-1EA
3DXMAX™ CFR-PLA carbon fiber reinforced PLA 3D printing filament	2.85	3DXCFR004-1EA
3DXMAX™ CFR-ABS carbon fiber reinforced ABS 3D printing filament	1.75	3DXCFR003-1EA
3DXMAX™ CFR-ABS carbon fiber reinforced ABS 3D printing filament	2.85	3DXCFR001-1EA

Carbon Nanotube Reinforced Filaments

Weight = 1.65 lb spool

Description	Diameter (mm)	Prod. No.
3DXNANO™ ESD CNT-ABS carbon nanotube reinforced ABS 3D printing filament	1.75	3DXCNT001-1EA
3DXNANO™ ESD CNT-ABS carbon nanotube reinforced ABS 3D printing filament	2.85	3DXCNT002-1EA
3DXNANO™ ESD CNT-PETG carbon nanotube reinforced polyethylene terephthalate glycol copolymer 3D printing filament	1.75	3DXCNT003-1EA
3DXNANO™ ESD CNT-PETG carbon nanotube reinforced polyethylene terephthalate glycol copolymer 3D printing filament	2.85	3DXCNT004-1EA

Nylon/ABS Alloy

Weight = 1.1 lb spool

Color	Diameter (mm)	Prod. No.
black	1.75	3DXION001-1EA
blue	1.75	3DXION002-1EA
red	1.75	3DXION003-1EA
natural	1.75	3DXION004-1EA

PET+®

Weight = 1 lb spool

Color	Diameter (mm)	Prod. No.
forest green	1.75	900114-1EA
	3	900115-1EA
gold (goldenrod)	1.75	900116-1EA
	3	900117-1EA
orange (tangerine)	1.75	900118-1EA
	3	900119-1EA
light brown (almond)	1.75	900120-1EA
	3	900121-1EA
ruby	1.75	900122-1EA
	3	900123-1EA
blue (sapphire)	1.75	900124-1EA
	3	900125-1EA

FlexSolid

Weight = 1 lb spool

Color	Diameter (mm)	Prod. No.
clear	1.75	900126-1EA
	2.85	900127-1EA
	3	900128-1EA

3D Printing UV Curable Resins

For a complete list of available materials, visit aldrich.com/3dp.

Name	Color	Size	Prod. No.
MS Resin®	blue	1 L	900129-1EA
	black	1 L	900130-1EA
	white	1 L	900132-1EA
	red	1 L	900133-1EA
	red (LittleRP red)	1 L	900134-1EA
Vorex®	black	500 mL	900136-1EA
	clear	500 mL	900138-1EA
	gray (grey)	500 mL	900139-1EA
	orange	500 mL	900135-1EA
	white	500 mL	900137-1EA
CastSolid® resin	yellow (translucent)	500 mL	900140-1EA

HAVE YOU MISSED OUR RECENT ISSUES?

- Vol. 11 No. 1: Next Generation Nanomaterials for Energy and Electronics (RYO)
- Vol. 10 No. 4: Biomaterials for Tissue Engineering (RVR)
- Vol. 10 No. 3: Alternative Energy Generation and Storage (RRB)
- Vol. 10 No. 2: Graphene and Carbon Materials (ROM)
- Vol. 10 No. 1: 10th Anniversary Issue—Materials that Matter (RQJ)
- Vol. 9 No. 4: Materials for Energy Harvesting and Storage (REO)

To view a complete library of issues or to subscribe to our newsletter, visit

aldrich.com/materialmatters



3D PRINTABLE CONDUCTIVE NANOCOMPOSITES OF PLA AND MULTI-WALLED CARBON NANOTUBES



Vincent Hughes, Ilyass Tabiai, Kambiz Chizari, Daniel Therriault*
Laboratory for Multiscale Mechanics (LM²)
École Polytechnique Montréal, QC H3T1J4, Canada
*Email: daniel.therriault@polymtl.ca

Introduction

A nanocomposite is typically defined as a mixture between a host material (e.g., polymer matrix) and nanofillers with at least one dimension of less than 100 nm. The addition of nanoparticles to a host material very often leads to significant improvements in material properties (e.g., mechanical, electrical, thermal) at relatively small loadings. The utilization of nanocomposites is being increasingly reported in a wide variety of fields including electronics,^{1,2} sporting goods,³ and aerospace.^{4,5} Some of the most commonly studied nanomaterials include carbon nanotubes, nanowires, buckyballs, graphene, metal particles, and quantum dots. Nanofillers can be used to transform an insulating material such as a polymer into a highly conductive material through the use of percolation pathways generated by the nanoparticles. Percolation pathways are routes in which a current can pass through the material. The size of the percolation pathway is often dependent upon nanoparticle characteristics such as aspect ratio and their alignment within the host matrix. As a host material, polymer matrices are widely used due to their ease of processability, low cost, and light weight. The addition of nanofillers into a polymer matrix comes with various challenges and difficulties including processing problems, dispersion and alignment complications, longer lead times, and higher overall cost.

The fabrication of nanocomposite structures through additive manufacturing is extremely promising for a myriad of applications such as tissue engineering scaffolds^{6,7} and liquid⁸ or strain sensors.⁹ Additive manufacturing (also referred to as three-dimensional (3D) printing) consists of joining materials to make complicated objects from a 3D computer-aided-design (CAD) model in a layer-by-layer fashion. Extrusion-based 3D printing methods create 3D structures by extruding material from a small diameter nozzle and depositing it onto a printing platform. This technique extrudes the material in a low viscosity state and solidifies post-extrusion. Two extrusion-based methods appropriate to the manufacture of nanocomposite thermoplastics are fused-deposition modeling (FDM)¹⁰ and solvent-cast printing.¹¹

FDM uses heat to melt the fabrication material and is a widely used method for the 3D printing of thermoplastics. The addition of nanoparticles to thermoplastic resin is known to increase the material viscosity to the point where clogging can occur more frequently within the nozzle even at high temperatures. Instead of using heat to soften the thermoplastic material, solvent-cast printing uses a solvent to dissolve the material and produce a printable ink solution at room temperature. This ink solution is extruded through a micro nozzle under constant applied pressure; the solution rapidly transitions from liquid-like to a solid-like structure due to fast evaporation of the solvent in air. This steep rigidity gradient makes conventional layer-by-layer printing possible but also provides the additional ability to fabricate freeform self-supporting curved shapes, such as reported by Guo, et al.¹² (Figure 1), which is not possible when printing via FDM. This, along with no material degradation due to heat, makes the solvent-cast process very encouraging as a 3D printing method.

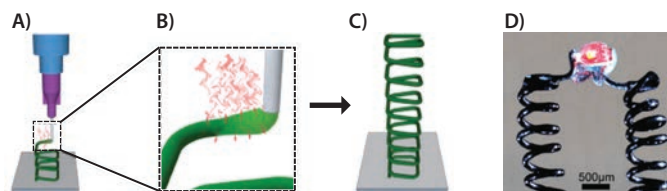


Figure 1. Solvent-cast 3D printing of freeform structures. **A)** Schematic representation of the process.¹² The solution is extruded from the syringe barrel through the nozzle. **B)** Close-up view of rapid solvent evaporation.¹² **C)** Example of freeform structure fabricated from this process.¹² **D)** LED bulb lit up by using 3D-printed freeform spirals made out of PLA and 5 wt% loading of MWCNT using the solvent-cast process.¹³

Here we present the solvent-cast printing of thin nanocomposite fibers made of thermoplastic poly(lactide) acid (PLA) reinforced with multi-walled carbon nanotubes (MWCNTs). PLA is suitable for this method because it is a widely available, low-cost thermoplastic that is biocompatible and biodegradable with good processability. MWCNTs are nanoparticles with large aspect ratios that exhibit good mechanical,¹⁴ electrical,¹⁵ and thermal¹⁶ properties. The solvent used to create a dilute ink solution of PLA/MWCNT is dichloromethane (DCM), chosen because of its ability to dissolve PLA and its low boiling point (39.6 °C). This article explores the methodology used for 3D printing nanocomposite fibers of PLA/MWCNT using the solvent-cast method. The steps include (1) the nanocomposite ink fabrication, (2) the solvent-cast printing process, and (3) the characterization of the printed fibers. This research shows the strong potential of 3D printing as a novel method for manufacturing nanocomposites with promising applications as reinforced structural parts, flexible electronics, electromagnetic shielding grids, and liquid sensors.

Experimental Method

Nanocomposite Fabrication

The MWCNTs (*Nanocyl NC7000*) are dispersed within PLA (*PLA 4032D*, *Natureworks LLC*) with a ball mill mixer method (*SPEX Sample Prep 8000M Mixer/Mill*).¹⁷ First, PLA is mixed with the solvent DCM to create a 10 wt% mixture and allowed to mix for 24 h for full dissolution. The PLA/DCM mixture is poured into a ball mill container with the desired amount of MWCNTs. We investigated the loading of MWCNTs of 0, 5, 10, and 20 wt%. The container is placed into the ball mill machine for 15 min to allow for proper dispersion of the nanofillers within the polymer matrix. Afterward, the mixture is left to dry for 24 h. After the solvent fully evaporates, the dry ink mixture is removed from the container and weighed. DCM is added at an amount based on the desired wt% of MWCNTs to this dry nanocomposite to yield a PLA/DCM concentration in the range of 25 to 30%. The mixture is left for 24 h to achieve full dissolution.

Solvent-cast 3D Printing

The nanocomposite ink is poured into a syringe barrel connected to a micronozzle mounted onto the head of a computer-controlled dispensing robot (*I&J2200-4*, *I&J Fisnar*). The extrusion pressure was controlled by a pressure regulator (*HP-7X*, *EFD*). The pressure ranged from 200–500 kPa depending on the desired linear flow rate of the ink coming out of the micronozzle, the nozzle size, and the nanocomposite ink concentration (i.e., viscosity of the ink). Continuous cylindrical fibers were extruded at 0 wt% CNT with a 150 μm inner diameter micronozzle, 5 wt% and 10 wt% with 200 μm and 20 wt% with 330 μm tip. The fibers were extruded onto a platform and left to dry for 10 min, then stored in airtight containers before performing subsequent characterization measurements.

Shrinkage Ratio Measurements

We defined the shrinkage ratio as the actual diameter of the fibers over the printing nozzle inner diameter. The fibers printed were cut into six 60-mm long sections for each MWCNT wt% and nozzle tip diameter. The actual diameter of the fibers was measured through digital image analysis taken with an optical microscope (*Olympus, BX61*). The diameter of each 60 mm fiber is measured at twelve different positions spaced by about 5 mm. An average diameter value for each fiber is calculated.

Density Measurements

The density of the fibers was measured using a helium pycnometer (*Micromeritics, AccuPyc II 1340*). The mass of the fibers was measured first and input into the pycnometer, which then measured the density ten times. An average was calculated. The measurement was performed for the fibers at 0, 10, and 20 wt% PLA/MWCNTs concentrations.

Conductivity Measurements

The conductivity measurements of the printed fibers were performed using a two-point probe method. The applied electrical current varied from 1 to 5 mA using a *Kiethley 6221* current source. The volume conductivity was calculated from the resistance values resulting from the two-point probe measurements and by knowing the length and diameter of each fiber. Measurements were done on each combination of MWCNT (0, 5, 10, and 20 wt%) and nozzle diameter (150, 200, 330 μm) at least six times.

Tensile Mechanical Measurements

Each fiber was mounted in the *Insight® MTS* electromechanical testing machine equipped with a 1 kN load cell and tested according to the ASTM D3822 standard test method for tensile properties of single textile fibers. Each combination of MWCNT percentage and nozzle diameter was tested at least three times.

Results and Discussion

Conductivity Results

Figure 2 shows the electrical conductivity of the 3D-printed nanocomposite fibers with respect to the MWCNT loadings. Pure PLA experiences no conductivity as expected. Increasing the MWCNT wt% from 5 to 20 causes the conductivity to go from 39.7 to 1,206 S/m, corresponding to a $\sim 3,000\%$ increase. This important conductivity is mainly attributed to the numerous particle-to-particle interactions, which increases the number of percolation pathways within the material. The conductivity of our material at 20 wt% performs extremely well against other polymer nanocomposites (**Figure 2B**) with the closest being 400 S/m for 3D printable nanocomposite of rubber/silver (Ag).¹⁸ Increasing the MWCNT wt% past 20% increases the conductivity; however, the increase in viscosity makes the printing process significantly harder.

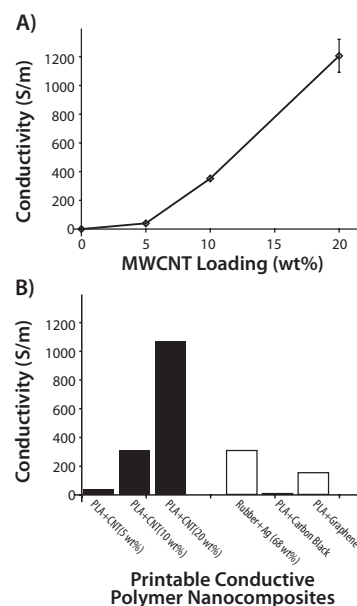


Figure 2. A) Conductivity of PLA/MWCNT fibers (wt%/nozzle diameter (μm) = 0/150; 5/200; 10/200; 20/330). B) Comparison of the conductivity of the 5, 10, and 20 wt% MWCNT (shaded bar charts) compared to other conductive polymer composites.^{18,19,20}

Tensile Mechanical Measurements

Figure 3 shows the mechanical properties of the nanocomposite fibers along with the shrinking and density measurements. **Figure 3A** shows the stress-strain curves of the pure PLA and the three MWCNT loadings. The measurements show a much lower strain-at-break when adding MWCNTs. The values change from 0.239 at pure PLA to 0.058 at 5 wt%, 0.046 at 10 wt%, and 0.009 at 20 wt% MWCNT, the largest drop being at 20 wt% with a 96% decrease in the strain-at-break from pure PLA. The tensile strength at pure PLA is 44 MPa; 5 and 10 wt% increases to 58 MPa and 56 MPa (31% and 27% improvement), respectively. The tensile strength at 20 wt% decreases from pure PLA by 28% to 32 MPa. Pure PLA has a ductile behavior with a large elongation at failure. Therefore, it is expected that the addition of MWCNTs would reduce the strain-at-break and make the material more brittle. The increase in tensile strength is also anticipated due to the covalent sp^2 bonds formed between the individual carbon atoms, which make carbon nanotubes one of the strongest and stiffest materials ever discovered.²¹ The decrease in tensile strength for the 20 wt% could be due to the weak van der Waals bonding of PLA-CNT. By increasing the loading of MWCNTs to 20 wt%, the stronger crosslinked bonds within the PLA are replaced by weaker bonds. PLA-CNT bonds are not as entangled, so the whole structure falls apart more easily at lower stress.

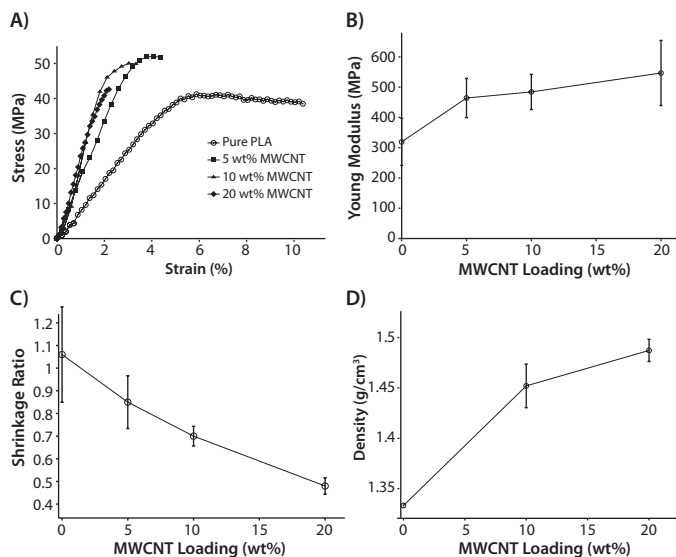


Figure 3. Mechanical results of the printed nanocomposite fibers (wt%/nozzle diameter (μm) = 0/150; 5/200; 10/200; 20/330). **A)** Stress-at-Strain curve of printed fibers. **B)** Plot of Young's Modulus against MWCNT loading. **C)** The calculated shrinkage ratios of each printed fiber. **D)** Helium pycnometer density measurements for pure PLA and reinforced MWCNT nanocomposite fibers.

Figure 3B presents the Young's Modulus for the different printed fibers. The modulus increases from 351 MPa for the pure PLA to 546 MPa for the 20 wt% fiber, corresponding to a 55% increase. It is possible that the extrusion of the ink inside the small nozzle helps the alignment of the nanotubes in the fibers, which would affect the resulting properties of the material.²²

Figure 3C displays the shrinkage ratio of PLA/MWCNTs for each MWCNT wt%. The plot clearly shows increasing shrinkage with higher loadings of MWCNT, whereas pure PLA actually increased in size by 6%. Maximum shrinkage occurred at 20 wt% and fiber diameter shrank 52%. The increased shrinkage is most likely related to the amount of DCM in the mixture. More solvent is needed at higher nanofiller concentrations to achieve suitable viscosity for printing. It is necessary to know this shrinkage so that the geometrical changes can be anticipated and correctly planned for the 3D printing of microstructures. **Figure 3D** shows the density with increasing MWCNT wt%. The density was measured at 0, 10, and 20 wt% of MWCNT and found to be 1.33, 1.452, and 1.48 g/cm³, respectively. Linear interpolation was used to find 5 wt% MWCNT of 1.391 g/cm³. The increasing density is directly related to the higher loadings of MWCNTs. This data will be useful for mechanical modeling purposes of larger structures made out of these 3D printed fibers.

Conclusion

In this work, the solvent-cast 3D printing technique is used to fabricate nanocomposite materials made of PLA and 5, 10, and 20 wt% MWCNTs concentrations. The addition of the nanotubes significantly affects the properties of the host material while preserving a very good solvent-cast printability. The best improvement was observed for the electrical conductivity where a maximum of 1,206 S/m at 20 wt% MWCNT was measured. To the best of our knowledge, this conductivity is superior to all the current printable commercial polymer-based composite materials. In addition to outstanding electrical properties, the nanocomposite material exhibits better stiffness than the pure PLA. However, the more electrically conductive fibers show a significant decrease of the strain-at-break making the fibers slightly more fragile. The tensile strength increased to 58 MPa for the 5 wt% fiber while it decreased for the 20 wt% MWCNT. The decrease may be attributed to the poor van der Waals bonding between PLA-CNT.

This study shows that it is possible to 3D print highly conductive polymer nanocomposites. While more work is needed to print more complex 3D structures, these materials have the potential to produce finished products in many niche applications. The high conductivity achieved opens the door for on-the-fly 3D-printed electrical components. 3D-printable conductive inks can be further enhanced when combined with other materials for integrated functionality (embedded sensors, EMI shielding, tactile surfaces). This research provides only a small insight into the possibilities enabled by 3D printing. The endless opportunities will only be realized with further work and future collaboration among other fields of science and technology.

References

- (1) Bae, S.; Kim, H.; Lee, X.; Xu, X.; Park, J.; Zheng, Y. *Nature Nanotech.* **2010**, *5*(8), 574-578.
- (2) Jiang, G. *Appl. Mech. Mater.* **2014**, 484-485, 114-117.
- (3) Nogi, M.; Yano, H. *Adv. Mater.* **2008**, *20*(10), 1849-1852.
- (4) Wu, N. *J. Aeronaut. Aerospace Eng.* **2012**, *01*(04).
- (5) Njuguna, J.; Pielichowski, K. *Adv. Eng. Mater.* **2003**, *5*(11), 769-778.
- (6) Farahani, R. D.; Dubé, M.; Therriault, D. *Adv. Mater.* **2016**, doi:10.1002/adma.201506215
- (7) Karageorgiou, V. D. *Biomaterials* **2005**, *26*(27), 5474-5491.
- (8) Guo, S.; Yang, X.; Heuzey, M.; Therriault, D. *Nanoscale* **2015**, *7*(15), 6451-6456.
- (9) Farahani, R.; Dalir, H.; Le, Borgne V.; Gautier, L.; El Khakani, M.; Lévesque, M. et al. *Nanotechnology* **2012**, *23*(8), 085502.
- (10) Leigh, S.; Bradley, R.; Purcell, C.; Billson, D.; Hutchins, D. *PLoS ONE* **2012**, *7*(11), e49365.
- (11) Farahani, R.; Chizari, K.; Therriault, D. *Nanoscale* **2014**, *6*(18), 10470.
- (12) Guo, S.; Heuzey, M.; Therriault, D. *Langmuir*. **2014**, *30*(4), 1142-1150.
- (13) Guo, S.; Yang, X.; Heuzey, M.; Therriault, D. *Nanoscale* **2015**, *7*(15), 6451-6456.
- (14) Treacy, M. M. J.; Ebbesen, T. W.; Gibson, J. M. *Nature* **1996**, *381*, 678-680.
- (15) Ebbesen, T. W.; Lezec, H. J.; Hiura, H.; Bennett, J. W.; Ghaemi, H. F.; Thio, T. *Nature* **1996**, *382*, 54-56.
- (16) Berber, S.; Kwon, Y. K.; Tománek, D. *Phys. Rev. Lett.* **2000**, *84*, 4613-4616.
- (17) Chizari, K.; Therriault, D. In *Fabrication of Conductive Microfilaments and Liquid Sensor from CNTs/PLA Nanocomposites*, Design, Manufacturing and Applications of Composites Tenth Workshop 2014: Proceedings of the Tenth Joint Canada-Japan Workshop on Composites, August 2014, Vancouver, Canada, DEStech Publications, Inc: **2015**; p 214.
- (18) Blackmagic3D. Conductive Graphene 3D Printing PLA Filament. URL <http://www.blackmagic3d.com/ProductDetails.asp?ProductCode=GRPHN%2D175>
- (19) Strümpfer, R.; Glatz-Reichenbach, J. *J. Electroceram.* **1999**, *3*, 329-346. doi:10.1023/A:1009909812823
- (20) ProtoPlant, Composite PLA - Electrically Conductive PLA. URL <https://www.proto-pasta.com/products/conductive-pla>
- (21) Salvétat, J.; Bonard, J.; Thomson, N.; Kulik, A.; Forró, L.; Benoit, W.; et al. *App. Phys. A-Mater.* **1999**, *69*(3), 255-260.
- (22) Thostenson, E.; Chou, T. J. *Phys. D: Appl. Phys.* **2002**, *35*(16), L77-L80.

Carbon Nanotubes

For a complete list of available materials, visit aldrich.com/cnt.

Single-walled Carbon Nanotubes

Production Method	Dimensions	Purity	Prod. No.
CoMoCAT® Catalytic Chemical Vapor Deposition (CVD) Method (6,5) chirality	diameter 0.7-0.9 nm (by fluorescence)	≥93% (carbon as SWNT)	773735-250MG 773735-1G
	diameter 0.7-0.9 nm (by fluorescence) L ≥700 nm	≥77% (carbon as SWNT)	704148-250MG 704148-1G
CoMoCAT® Catalytic Chemical Vapor Deposition (CVD) Method (7,6) chirality	diameter 0.7-1.1 nm L 300-2,300 nm (mode: 800 nm; AFM)	≥77% (carbon as SWNT)	704121-250MG 704121-1G
CoMoCAT® Catalytic Chemical Vapor Deposition (CVD) Method	diameter 0.6-1.1 nm	>95% (carbon as SWCNT)	775533-250MG 775533-1G
	diameter 0.7-1.4 nm	≥80.0% (carbon as SWNT)	724777-250MG 724777-1G
	diameter 0.7-1.3 nm L 450-2,300 nm (mode: 800 nm; AFM)	≥70% (carbon as SWNT)	704113-250MG 704113-1G
Catalytic Carbon Vapor Deposition (CCVD) Method	average diameter 2 nm L 3 μm	>70%	755710-250MG 755710-1G
Electric Arc Discharge Method	diameter 1.2-1.7 nm L 0.3-5 μm	30% (Metallic) 70% (Semiconducting)	750492-100MG
	diameter 1.2-1.7 nm L 0.3-5 μm	30% (Metallic) 70% (Semiconducting)	750514-25MG
	diameter 1.2-1.7 nm L 0.3-5 μm	2% (Metallic) 98% (Semiconducting)	750522-1MG
	diameter 1.2-1.7 nm L 0.3-5 μm	98% (Metallic) 2% (Semiconducting)	750530-1MG
	D × L 2-10 nm × 1-5 μm (bundle dimensions) 1.3-1.5 nm (individual SWNT diameter)	40-60 wt. %	698695-1G 698695-5G

Single-walled Carbon Nanotube Inks

Form	SWCNT Concentration	Viscosity	Sheet Resistance	Prod. No.
dispersion in H ₂ O (black liquid)	0.20 ± 0.01 g/L (by Absorbance at 854 nm)	~1.0 mPa.s	<400 Ω/sq (by 4-point probe on prepared film by spray)	791490-25ML 791490-100ML
	1.00 ± 0.05 g/L (by Absorbance at 854 nm)	3.0 mPa.s (at 10 s ⁻¹ shear rate)	<600 Ω/sq (at 85% VLT (ohm/sq), by 4-point probe on prepared film by spray)	791504-25ML 791504-100ML
viscous liquid (black)	1 mg/mL	17.7 Pa.s at 25 °C (at 10 s ⁻¹ shear rate)	<1,000 Ω/sq (by 4-point probe on prepared, at 87.5% VLT (ohm/sq))	792462-25ML 792462-100ML

Double-walled Carbon Nanotubes

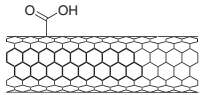
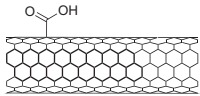
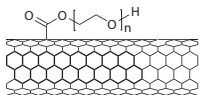
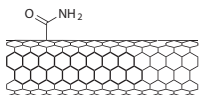
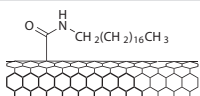
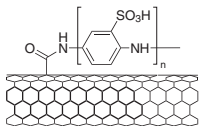
Production Method	Dimensions	Purity	Prod. No.
Catalytic Carbon Vapor Deposition (CCVD) Method	avg. diam. × L 3.5 nm × >3 μm (TEM)	Metal Oxide ≤10% TGA	755141-1G
	avg. diam. × L 3.5 nm × 1-10 μm (TEM)	Metal Oxide <10% TGA	755168-1G
Chemical Vapor Deposition (CVD) Method	O.D. × I.D. × L 5 nm × 1.3-2.0 nm × 50 μm	50-80%	637351-250MG 637351-1G

Multi-walled Carbon Nanotubes

Production Method	Description	Purity	Prod. No.
CoMoCAT® Catalytic Chemical Vapor Deposition (CVD) Method	O.D. × I.D. × L 10 nm ±1 nm × 4.5 nm ±0.5 nm × 3~6 μm (TEM)	≥98% carbon basis	773840-25G 773840-100G
	O.D. × L 6-9 nm × 5 μm diam. 6.6 nm (median) diam. 5.5 nm (mode)	>95% (carbon)	724769-25G 724769-100G
	O.D. × I.D. × L 10 nm × 4.5 nm × 4 μm Aspect ratio (L/D) 350-550 Tubes typically have 6-8 tube walls.	70-80% (carbon)	791431-25G 791431-100G
Catalytic Carbon Vapor Deposition (CCVD) Method	avg. diam. × L 9.5 nm × <1 μm (TEM) thin and short	Metal Oxide <5% TGA	755117-1G
	avg. diam. × L 9.5 nm × 1.5 μm (TEM) thin	Metal Oxide <5% TGA	755133-5G

Production Method	Description	Purity	Prod. No.
Chemical Vapor Deposition (CVD) Method	O.D. \times L 6-13 nm \times 2.5-20 μ m 12 nm (average diameter, HRTEM) 10 μ m (average length, TEM)	>98% carbon basis	698849-1G
	D \times L 110-170 nm \times 5-9 μ m	>90% carbon basis	659258-2G 659258-10G
Electric Arc Discharge Method	O.D. \times L 7-12 nm \times 0.5-10 μ m powdered cylinder cores	20-30% MWCNT basis	406074-500MG 406074-1G 406074-5G
	O.D. \times L 7-15 nm \times 0.5-10 μ m as-produced cathode deposit	>7.5% MWCNT basis	412988-100MG 412988-2G 412988-10G
Plasma-Enhanced Chemical Vapor Deposition (PECVD) Method	diam. \times L 100-150 nm \times 30 μ m (SEM) vertically aligned on silicon wafer substrate	>95 atom % carbon basis (x-ray)	687804-1EA

Functionalized Nanotubes

Structure	Name	Purity (%)	Dimensions (D \times L)	Production Method	Prod. No.
	Carbon nanotube, single-walled, carboxylic acid functionalized	>90	4-5 nm \times 0.5-1.5 μ m (bundle dimensions)	Electric Arc Discharge Method	652490-250MG 652490-1G
	Carbon nanotube, multi-walled, carboxylic acid functionalized	>80	9.5 nm \times 1.5 μ m	Catalytic Carbon Vapor Deposition (CCVD) Method	755125-1G
	Carbon nanotube, single-walled, poly(ethylene glycol) functionalized	>80	4-5 nm \times 0.5-0.6 μ m (bundle dimensions)	Electric Arc Discharge Method	652474-100MG
	Carbon nanotube, single-walled, amide functionalized	>90	4-6 nm \times 0.7-1.0 μ m (bundle dimensions)	Electric Arc Discharge Method	685380-100MG
	Carbon nanotube, single-walled, octadecylamine functionalized	80-90	2-10 nm \times 0.5-2 μ m (bundle dimensions)	Electric Arc Discharge Method	652482-100MG
	Carbon nanotube, single-walled, polyaminobenzene sulfonic acid functionalized	75-85	1.1 nm \times 0.5-1.0 μ m (bundle dimensions)	Electric Arc Discharge Method	639230-100MG

CARBON NANOTUBE 3D PRINTING FILAMENTS

3DXNANO™ ESD Carbon Nanotube (CNT) Printing Filaments are used in critical applications that require electrostatic discharge (ESD) protection and a high level of cleanliness. The compounded filaments are formulated with premium Acrylonitrile Butadiene Styrene (ABS) or Polyethylene Terephthalate Glycol (PETG) resin and multi-walled CNTs in the presence of dispersion modifiers, resulting in a filament with excellent printing characteristics and consistent ESD properties.

Properties of 3DXNANO™ ESD 3D Printing Filaments

- Consistent surface resistivity (target $1.0 \times 10^7 - 10^9 \Omega$)
- Amorphous polymers – low and near isotropic shrinkage
- ABS suitable for water-based conformal coatings
- Low moisture absorption of PETG
- PETG preferred for solvent-based conformal coatings
- Excellent retention of base-resin ductility due to low loading rate of CNTs needed to achieve ESD
- Ultra-low particulate contamination vs. carbon black compounds



Name	Diameter (mm)	Prod. No.
3DXNANO™ ESD CNT-ABS 3D printing filament	1.75	3DXCNT001
	2.85	3DXCNT002
3DXNANO™ ESD CNT-PETG 3D printing filament	1.75	3DXCNT003
	2.85	3DXCNT004

For the complete nanomaterials offering, visit
[aldrich.com/3dp](https://www.aldrich.com/3dp)

NANOPARTICLE-BASED ZINC OXIDE ELECTRON TRANSPORT LAYERS FOR PRINTED ORGANIC PHOTODETECTORS



Gerardo Hernandez-Sosa,^{1,2*} Ralph Eckstein,^{1,2} Tobias Rödlmeier,^{1,2} Uli Lemmer^{1,2,3}

¹Lichttechnisches Institut, Karlsruher Institut für Technologie,

Engesserstrasse 13, 76131 Karlsruhe, Germany

²InnovationLab, Speyerer Str. 4, Heidelberg, Germany

³Institut für Mikrostrukturtechnik, Karlsruher Institut für Technologie,

Hermann-von-Helmholtz-Platz 1, 76344 Eggenstein-Leopoldshafen, Germany

*Email: gerardo.sosa@kit.edu

Introduction

Recent progress in the area of solution-processed functional materials has led to the development of a variety of thin-film optoelectronic devices with significant promise in the industrial and consumer electronics fields.^{1,2} These devices are becoming core technologies for the development of novel applications in sensing,³ energy harvesting,⁴ and energy conversion, exhibiting a unique combination of mechanical flexibility and light weight.⁵ Optical sensor research is growing in the area of organic photodiodes, with a special focus on the development of high-performance multilayer device architectures printed on a variety of substrates.^{6,7} We present the fabrication of printed organic photodiodes (OPDs) based on bulk-heterojunction (BHJ) active materials utilizing zinc oxide (ZnO) hole blocking layers deposited from nanoparticle (NP)-based ink. In contrast to sol gel or precursor-based layer deposition, the use of NPs offers great benefits with regard to processability and, in particular, the ability to precisely adjust the electronic and optical properties of the NPs without influence from the required conditions of thin film deposition.

Figures of Merit of Photodetectors

Organic BHJ photodetectors and solar cells generally have the same device architecture and material set. However, they differ in application focus which requires the optimization of different figures of merit. While solar cells are generally characterized by the short circuit current density (J_{sc}), open circuit voltage (V_{oc}), fill factor (FF), and device efficiency (η), photodiodes are characterized by the current On–Off ratio in reverse bias, specific detectivity (D^*), bandwidth (BW), and spectral responsivity (SR). SR is given in amperes per watt (A/W) and is analogous to the external quantum efficiency (EQE) in solar cells, as seen in **Equation 1**:

$$SR = \frac{I_{ph}}{P_{opt}(\lambda)} = EQE \cdot \frac{\lambda \cdot q}{h \cdot c} \quad (1)$$

where I_{ph} is the generated photocurrent per wavelength λ , q is the electron charge, c the speed of light, and h the Planck constant.

Unlike solar cells, photodiodes are generally operated in reverse bias in order to achieve a larger collection of photo-excited carriers. The On–Off ratio of photodiodes is defined as the ratio between the measured current under illumination and dark conditions at a certain bias voltage. The dark current density (J_{dark}) can be used to estimate the electrical noise (S_{noise}), which is dominated by the shot noise of the OPDs, as seen in **Equation 2**. A lower S_{noise} compared to the obtained SR will result in a higher D^* as evident from **Equation 3**. D^* is a figure of merit of photodetectors which characterizes the smallest detectable signal of the device.

$$S_{noise} = \sqrt{2 \cdot q \cdot J_{dark} \cdot \Delta f \cdot A} \quad (2)$$

$$D^* = \frac{SR \cdot \sqrt{\Delta f \cdot A}}{S_{noise}} = \frac{SR}{\sqrt{2 \cdot q \cdot J_{dark}}} \quad (3)$$

The dynamic response of the photodiode is characterized by its BW , which can be obtained by a transient photocurrent measurement or by varying the frequency of the excitation source. BW is usually defined by the cut-off frequency at –3 dB, which corresponds to a power drop of ~50%.

Results of Fully Printed Photodetectors

In practice, the main leverage for increasing the On–Off ratio and, consequently, D^* of a photodetector is the reduction of the dark current. This can be achieved by introducing interlayers that selectively block electrons in the device architecture in order to avoid charge recombination at the active layer/electrode interface and simultaneously adjusting the energy levels of the electrode to the active material. ZnO NPs have shown exceptional electron transport properties within optoelectronic devices.^{8,9} The photodiodes presented in this work were fabricated in an inverted device architecture onto indium-doped tin oxide (ITO)-covered glass or PET substrates. The electron transport layer (ETL) using ZnO NP dispersions was fabricated by spin casting, inkjet printing, and aerosol printing. A thermal treatment at 120 °C for 5 minutes was applied to fully dry the ETL. The active material comprising P3HT (poly(3-hexylthiophene-2,5-diy)) (**Prod. Nos. 698997** and **698989**) and PCBM ([6,6]-phenyl C₆₁ butyric acid methyl ester) (**Prod. No. 684457**) diluted in dichlorobenzene (40 g/L) was blended in a ratio of 1:0.9 and was spin cast, resulting in a ~200 nm thick layer. A 20 nm thick poly(3,4-ethylenedioxythiophene) polystyrene sulfonate (PEDOT:PSS) layer was spin cast and used as the hole transport layer (HTL). Afterward, the samples were transferred to a nitrogen-filled glovebox and thermally treated at 145 °C for 15 minutes on a hotplate in order to remove humidity from the PEDOT:PSS layer and improve BHJ morphology.

The 100 nm thick silver top electrode was thermally evaporated through a shadow mask in a vacuum system with a base pressure of 10^{-7} mbar. For the aerosol-printed OPDs, an active layer of poly([4,8-bis[(2-ethylhexyl)oxy]benzo[1,2-b:4,5-b']dithiophene-2,6-diyl]{3-fluoro-2-[(2-ethylhexyl)carbonyl]thieno[3,4-b]thiophenediyl}) (PTB7, Prod. No. 772410) was blended with [6,6]-Phenyl- C_{71} -butyric acid methyl ester (PC70BM, Prod. No. 684465) using a ratio of 1:1.5 (10 g L^{-1} in 1,2-dichlorobenzene) with 3% volume of diiodooctane printed on top of a PEDOT:PSS/AZO cathode. The film was then dried in a vacuum (15 mbar) for 15 minutes. The conductive transparent top anode was aerosol-printed using a diluted PEDOT:PSS dispersion and finally dried in vacuum (15 mbar) in an antechamber, then transferred into a glovebox. All devices were encapsulated with an adhesive barrier foil to avoid the penetration of oxygen and moisture into the device.

The OPD architecture and the relative energy level arrangement of the materials is shown in Figure 1A. Atomic force microscope (AFM) measurements were conducted on inkjet and aerosol-jet printed ZnO nanoparticle layers on ITO as shown in Figure 1B. Inkjet-printed ZnO using N11 Jet (Prod. No. 808202) formulation and aerosol-jet printed ZnO using N11 Slot (Prod. No. 808199) produced the best results. Both techniques delivered a very homogeneous ZnO dense layer with a Root Mean Square (RMS) roughness on the order of 2.7 to 3 nm.

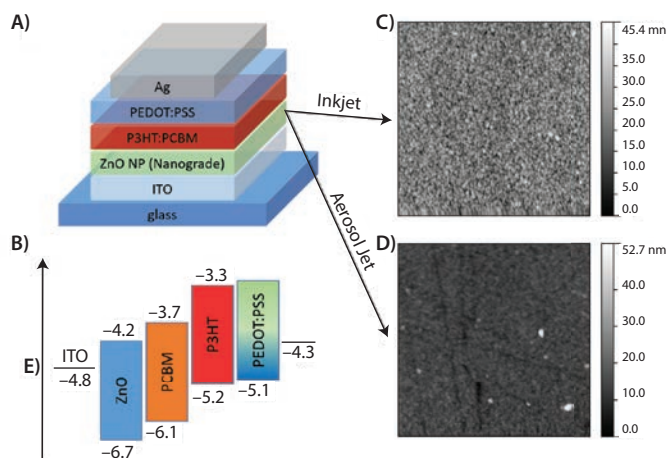


Figure 1. A) Inverted organic photodiode stack. B) Corresponding band diagram. AFM image ($10 \times 10 \mu\text{m}^2$) of C) inkjet-printed N11 Jet and D) aerosol-jet printed N11 Slot on ITO-covered glass.

The J-V characteristic of devices with spin cast (SC), inkjet (IJ), and aerosol (AJ) printed A) aluminium-doped ZnO (AZO) and B) ZnO nanoparticle-based layers are presented in Figure 2. The device characteristics can be found in Table 1. A dark current density on the order of 10^{-4} mA/cm^2 at -1 V was observed for the spin-cast AZO and ZnO layers, demonstrating the suitability of these ETLs for photodiode application. IJ-printed AZO layers show results as good as the spin-cast AZO layers; however, J_{dark} for AJ-printed ZnO, and IJ- or AJ-printed AZO-comprising devices is increased.

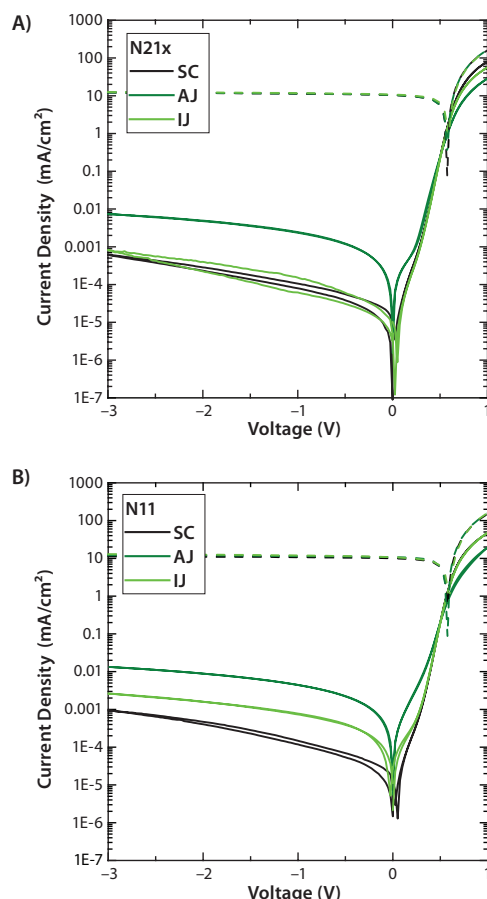


Figure 2. J-V curves of inverted stack comprising A) spin cast (SC) AZO (N21x), inkjet (IJ) (N21x Jet), and aerosol jet (AJ) (N21x slot) layers and B) for ZnO (N11, N11 Jet, N11 Slot), respectively.

This suggests that some low resistant pathways are formed during drying of the printed films. In both digital printing technologies, a sequential printing path is used. A local inhomogeneity of the surface energy on the ITO substrate can lead to incomplete wetting and even to pin holes in the ZnO layer. The layer thickness of the spin-cast ZnO and AZO layers is $\sim 30 \text{ nm}$, while the necessary thickness of the IJ and AJP ZnO/AJP layers is below 50 nm . In the case of inkjet printing, the layer thickness was adjusted by the drop spacing or the NP concentration in the ink. Film thicknesses of AJ-printed ZnO layers are adjusted through a variety of parameters including the mist density, printing velocity, atomizer, and sheath gas flows. Further information about the aerosol working principle can be found elsewhere.¹⁰ All devices showed solar cell efficiencies $>3\%$, with fill factors exceeding 53% as shown in Table 1.

Table 1. Inverted solar cell parameters of devices comprising SC, IJ, and AJ-printed ZnO and AZO layers.

Device	J_{sc} (mA/cm^2)	$J_{\text{dark}} @ -1 \text{ V}$ ($\mu\text{A/cm}^2$)	Efficiency (%)	Fill factor (%)
N21x SC	-10.3	-1.94	3.27	54.94
N21x IJ (Jet)	-10.8	-3.02	3.53	54.63
N21x AJ (slot)	-10.5	-41.00	3.23	53.79
N11 Sc	-10.0	-9.20	3.31	57.42
N11 IJ (Jet)	-10.7	-11.13	3.46	53.90
N11 AJ (slot)	-10.8	-64.80	3.56	57.53

Fully AJ-printed semi-transparent photodiodes are presented in **Figure 3**. The inverted device stack, shown in **Figure 3A**, comprises a transparent conductive PEDOT:PSS/AZO bottom electrode printed on PET foil. PTB7:PC70BM was used as the active material. Conductive PEDOT:PSS was AJ-printed in a similar manner as the top electrode. **Figure 3B** shows a device that achieved a 2 mm bending radius; smaller bending radii led to irreversible deformation of the device due to delamination of the barrier foils. The *EQE* and *SR* of the device under bending conditions and in normal state are shown in **Figure 3C**. In stress-free conditions the fully printed OPD showed an average *SR* of ~ 0.25 A/W from 400 to 700 nm at -3 V reverse bias. The bended device showed only a marginal reduction of $<5\%$. The D^* for both cases was found to be $\sim 10^{11}$ Jones, with *BW* on the order of 200 kHz.⁷

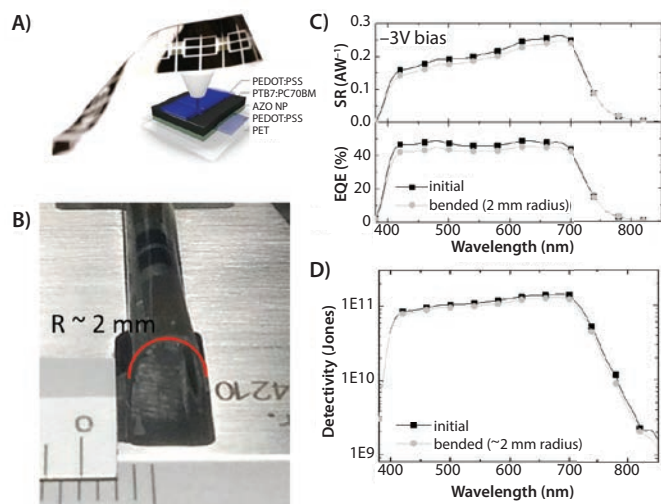


Figure 3. Fully AJ-printed organic photodiodes. **A)** Scheme of inverted stack, comprising a PEDOT:PSS/AZO anode and a PEDOT:PSS cathode. **B)** Flexible OPD on PET substrate at bending radius of 2 mm. **C)** Spectral response (*SR*) and *EQE* before and during bending at -3 V reverse bias. **D)** Specific detectivity (D^*) before and during bending at 2 mm radius. Adapted and reproduced with permission from Reference 7, ©2015 John Wiley & Sons Inc.

Nanoparticle Inks for Printing

For a complete list of available materials, visit aldrich.com/inks.

Zinc Oxide

Particle Size (nm)	Concentration (wt. %)	Viscosity (cP)	Work Function (eV)	Prod. No.
10-15	2.7 (crystalline ZnO in 2-propanol)	-	-	793361-5ML 793361-25ML
8-16	2.5 (crystalline ZnO in isopropanol)	1.6-2.6	-3.7 to -4.1	808253-10ML
	2.5 (crystalline ZnO in isopropanol and propylene glycol)	2.4-3.8	-4.1 to -4.5	807648-10ML
	2.5 (crystalline ZnO in isopropanol and propylene glycol)	2.4-3.7	-3.7 to -4.1	808199-10ML
	2.5 (crystalline ZnO in isopropanol and propylene glycol)	8-14	-4.1 to -4.5	807613-5ML
	2.5 (crystalline ZnO in isopropanol and propylene glycol)	8-14	-3.7 to -4.1	808202-5ML
2.5 (crystalline ZnO in α -terpineol)	26-36	-	-4.1 to -4.5	807621-10ML
7-17	2.5 (crystalline ZnO in α -Terpineol)	32-48	-3.7 to -4.1	808075-10ML

Conclusion

We have presented the properties of printed organic photodiodes utilizing ZnO nanoparticle-based ETLs. The ZnO nanoparticles allow low dark currents and specific detectivities comparable to spin cast devices, regardless of whether they were produced by AJ or IJ printing. We also showed that the devices can be processed on flexible substrates and can be operated under mechanical stress. These results highlight the applicability of nanoparticle-based inks to flexible printed thin-film electronics and the potential use of organic photodiodes as optical sensors manufactured by digital printing technologies.

Acknowledgment

The authors acknowledge financial support of the German Federal Ministry of Education and Research via project FKZ: 13N13691.

References

- (1) Punke, M.; Valouch, S.; Kettlitz, S. W.; Gerken, M.; Lemmer, U. *J. Lightwave Technol.* **2008**, *26*, 816–823.
- (2) Ho, C. K.; Robinson, A.; Miller, D. R.; Davis, M. J. *Sensors*. **2005**, *5*, 4–37.
- (3) Sprules, S. D.; Hart, J. P.; Pittson, R.; Wring, S. A. *Electroanal.* **1996**, *8*, 539–543.
- (4) Wöhrle, D.; Meissner, D. *Adv. Mater.* **1991**, *3*, 129–138.
- (5) Kaltenbrunner, M.; White, M. S.; Glowacki, E. D.; Sekitani, T.; Someya, T.; Sariciftci, N. S.; Bauer, S. *Nat Commun.* **2012**, *3*, 770.
- (6) Baeg, K. J.; Binda, M.; Natali, D.; Caironi, M.; Noh, Y. Y. *Adv. Mater.* **2013**, *25*, 4267–4295.
- (7) Eckstein, R.; Rödlmeier, T.; Glaser, T.; Valouch, S.; Mauer, R.; Lemmer, U.; Hernandez-Sosa, G. *Adv. Electron. Mater.* **2015**, *1*, 1500101.
- (8) Yang, T.; Cai, W.; Qin, D.; Wang, E.; Lan, L.; Gong, X.; Peng, J.; Cao, Y. *J. Phys. Chem. C* **2010**, *114* (14), 6849–6853.
- (9) Letellier, P.; Mayaffre, A.; Turmine, M. *J. Colloid Interface Sci.* **2007**, *314*, 604–614.
- (10) Eckstein, R.; Hernandez-Sosa, G.; Lemmer, U.; Mechau, N. *Org. Electron.* **2014**, *15*, 2135–2140.

Aluminum-doped Zinc Oxide

Particle Size (nm)	Concentration (wt. %)	Viscosity (cP)	Work Function (eV)	Prod. No.
<50 (BET)	2.5 (crystalline Al-doped ZnO (98 wt% ZnO; 2 wt% Al ₂ O ₃) in 2-propanol)	-	-	793388-5ML 793388-25ML
8-16	2.5 (crystalline Al doped ZnO (3.15 mol% Al) in mixture of alcohols)	1.7-2.7	-3.7 to -4.1	808237-10ML
	2.5 (crystalline Al doped ZnO (3.15 mol% Al) in 2-propanol)	1.9-3.1	-4.1 to -4.5	807729-10ML
	2.5 (crystalline Al doped ZnO (3.15 mol% Al) in 2-propanol and propylene glycol)	2.4-4.0	-4.1 to -4.5	807656-10ML
	2.5 (crystalline Al doped ZnO (3.15 mol% Al) in 2-propanol and propylene glycol)	2.5-3.7	-3.7 to -4.1	808164-10ML
	2.5 (crystalline Al doped ZnO (3.15 mol% Al) in 2-propanol and propylene glycol)	8-14	-3.7 to -4.1	808180-5ML
	2.5 (crystalline Al doped ZnO (3.15 mol% Al) in 2-propanol and propylene glycol)	8-14	-4.1 to -4.5	808172-5ML
	2.5 (crystalline Al doped ZnO (3.15 mol% Al) in α -terpineol)	25-37	-4.1 to -4.5	808210-10ML
	2.5 (crystalline Al doped ZnO (3.15 mol% Al) in mixture of alcohols)	32-48	-3.7 to -4.1	808229-10ML

Titanium Dioxide

Name	Particle Size (nm)	Concentration (wt. %)	Description	Prod. No.
Titania paste, active opaque	20 (active)	27.0	>99% anatase	791555-5G
	≤ 450 (scatter)			791555-20G
Titania paste, reflector	150-250 (scatter)	20.0	>99% anatase	791539-5G 791539-20G
Titania paste, transparent	20 (active)	19.0	>99% anatase	791547-10G
				791547-20G
Titanium dioxide	22-25 (BET)	16	nanocrystalline colloidal paste for transparent film	798495-25G
	18-20 (BET)	16	>95% anatase (XRD) nanocrystalline colloidal paste for transparent film	798509-25G
	22 and > 150 (BET)	16	>95% anatase (XRD) colloidal paste for opaque film	798517-25G
	18-20 (BET)	16	nanocrystalline colloidal paste for opaque film	798525-25G

Silver

Name	Particle Size (nm)	Concentration	Viscosity at 25 °C	Prod. No.
Silver, dispersion	≤ 10	50-60 wt. % in tetradecane	8-14 cP	736511-25G 736511-100G
	≤ 50	30-35 wt. % in triethylene glycol monomethyl ether	10-18 cP	736473-25G 736473-100G
	≤ 10	50-60 wt. % in tetradecane	7-14 cP	736503-25G 736503-100G
	≤ 50	30-35 wt. % in triethylene glycol monomethyl ether	10-18 cP	736465-25G 736465-100G
	≤ 50	30-35 wt. % in triethylene glycol monoethyl ether	10-18 cP	736481-25G 736481-100G
	Silver nanoparticle ink	115 (d_{90} (by Brookhaven)) 70 (d_{50} (by Brookhaven))	30 wt. % dispersion in ethylene glycol	28 cP
70 (d_{50}) 115 (d_{90})		50 wt. %	24 cP	796042-5G 796042-20G
<5 (20%) 200 (80%)		$\geq 75\%$	100,000-300,000 cP	735825-25G
Conductive silver printing ink, resistivity 30-35 $\mu\Omega/cm$	-	-	6,000-9,000 mPa.s	791903-10G 791903-20G
Conductive silver printing ink, resistivity 5-6 $\mu\Omega/cm$	-	-	13,000-17,000 mPa.s	791873-10G 791873-20G
Conductive silver printing ink, resistivity 9-10 $\mu\Omega/cm$	-	-	9,000-12,000 mPa.s	791881-10G 791881-20G
Reactive silver ink	-	-	10-12 cP	745707-25ML

Other Nanoparticles

Name	Particle Size (nm)	Concentration	Viscosity	Prod. No.
Molybdenum oxide nanoparticle ink	8-16	-	1-3 cP	900151-10ML
Platinum paste, screen printable	-	-	2,500-4,500 mPa.s	791512-20G
Tungsten oxide nanoparticle ink	11-21	2.5 wt. %	8 cP	807753-5ML
Tungsten oxide (WO _{3-x}) nanoparticle ink	<50 (BET)	2.5 wt. % in 2-propanol	-	793353-5ML 793353-25ML

Organic Conductive Inks

For a complete list of available materials, visit aldrich.com/conductiveink.

Name	Viscosity at 25 °C (cP)	Resistivity (Ω/cm)	Work Function (eV)	Prod. No.
Plexcore® OC AQ-1100 Organic Conductive Ink	4-7	500-5,000 (Film)	-5.6 ± 0.1 eV (Film)	805068-20ML
Plexcore® OC AQ-1200 Organic Conductive Ink	3.3-5.3	1,000-5,000 (Film)	-5.3 ± 0.1 eV (AC2, Film)	805785-20ML
Plexcore® OC AQ-1250 Organic Conductive Ink	3.3-5.5	400-5,000 (Film)	-5.3 ± 0.1 eV (AC2, Film)	805793-20ML
Poly(thiophene-3-[2-(2-methoxyethoxy)ethoxy]-2,5-diyl), sulfonated	4.0-10.0 (Brookfield)	500-3,000	-5.1 to -5.2	699780-25ML
Poly(thiophene-3-[2-(2-methoxyethoxy)ethoxy]-2,5-diyl), sulfonated	7-13 (Brookfield)	25-250	-5.1 to -5.2	699799-25ML

Ink Kits

For a complete list of available materials, visit aldrich.com/conductiveink.

Name	Application	Prod. No.
Organic photovoltaic ink system	Ready-to-use organic ink system for bulk heterojunction solar cells and spin coating.	711349-1KT
Organic photovoltaic ink system, PV 2000 kit	Ready-to-use organic ink system for bulk heterojunction solar cells and spin coating.	772364-1KT

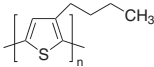
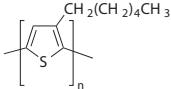
Poly(3,4-ethylenedioxythiophene):poly(styrenesulfonate) (PEDOT:PSS)

For a complete list of available materials, visit aldrich.com/pedot.

Description	Sheet Resistance (Ω/sq)	Viscosity	pH	Prod. No.
0.8% in H ₂ O, conductive inkjet ink	-	7-12 cP at 22 °C	1.5-2.5	739316-25G
1.1% in H ₂ O, neutral pH, high-conductivity grade	resistance <100 (>70% visible light transmission, 40 μm wet)	<100 cP at 22 °C	5-7	739324-100G
1.1% in H ₂ O, surfactant-free, high-conductivity grade	resistance <100 (<80% visible light transmission, 40 μm wet)	<100 cP at 22 °C	<2.5	739332-100G
1.0 wt. % in H ₂ O, high-conductivity grade	resistance 50-120	7-12 mPa.s at 22 °C (typical)	1.8-2.2	768642-25G
5.0 wt. %, conductive screen printable ink	resistance 50-150	30,000-90,000 mPa.s at 22 °C	1.5-2.0	768650-25G
dry re-dispersible pellets, high conductivity	sheet resistance <200 (by addition of 5% diethylene glycol)	-	-	900208-1G
high-conductivity grade	sheet resistance <200 (coating: 40 μm wet, drying: 6 min 130 °C)	<30 mPa.s at 20 °C	-	900181-100G
3.0-4.0% in H ₂ O, high-conductivity grade	resistance 1,500 (4 point probe measurement of dried coating based on initial 6 μm wet thickness.) resistance 500 (4 point probe measurement of dried coating based on initial 18 μm wet thickness.)	10-30 cP at 20 °C	1.5-2.5 at 25 °C (dried coatings)	655201-5G 655201-25G
2.8 wt % dispersion in H ₂ O, low-conductivity grade	-	<20 cP at 20 °C	1.2-1.8	560596-25G 560596-100G
dry re-dispersible pellets, dry re-dispersible pellets	resistance 200-450	-	-	768618-1G 768618-5G

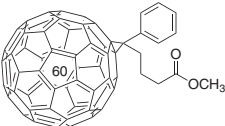
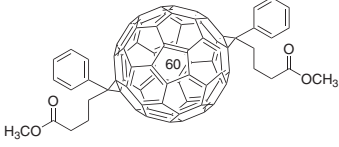
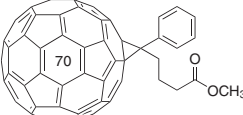
Polythiophene (PT)

For a complete list of available materials, visit aldrich.com/polythio.

Name	Structure	Regioregularity	Molecular Weight	Prod. No.
Poly(3-butylthiophene-2,5-diyl), P3BT		regioregular	M _w 54,000 (typical)	495336-1G
		regiorandom	-	511420-1G
Poly(3-hexylthiophene-2,5-diyl), P3HT		regioregular	average M _n 54,000-75,000	698997-250MG 698997-1G 698997-5G
		regioregular	average M _n 15,000-45,000	698989-250MG 698989-1G 698989-5G
		regioregular	-	445703-1G
		regiorandom	-	510823-1G

Fullerenes

For a complete list of available materials, visit aldrich.com/fullerene.

Structure	Name	Purity (%)	Prod. No.
	[6,6]-Phenyl C ₆₁ butyric acid methyl ester	>99.9	684457-100MG
	[6,6]-Phenyl C ₆₁ butyric acid methyl ester	>99.5	684449-100MG 684449-500MG
	[6,6]-Phenyl C ₆₁ butyric acid methyl ester	>99	684430-1G
	[6.6] Diphenyl C ₆₂ bis(butyric acid methyl ester) (mixture of isomers)	99.5	704326-100MG
	[6,6]-Phenyl C ₇₁ butyric acid methyl ester, mixture of isomers	99	684465-100MG 684465-500MG
	ICMA	97	753947-250MG
	ICBA	99	753955-250MG

Indium Tin Oxide (ITO) Coated Substrates

For a complete list of available materials, visit aldrich.com/ito.

Description	Dimension (L x W x thickness)	Surface Resistivity (Ω/sq)	Prod. No.
Indium tin oxide coated PET	1 ft x 1 ft x 5 mil	60	639303-1EA 639303-5EA
	1 ft x 1 ft x 5 mil	100	639281-1EA 639281-5EA
	1 ft x 1 ft x 5 mil	200	749745-1EA 749745-5EA
	1 ft x 1 ft x 5 mil	250	749761-1EA 749761-5EA
	1 ft x 1 ft x 5 mil	300	749796-1EA 749796-5EA
	1 ft x 1 ft x 7 mil	60	749729-1EA 749729-5EA
	1 ft x 1 ft x 7 mil	100	749737-1EA 749737-5EA
	1 ft x 1 ft x 7 mil	200	749753-1EA 749753-5EA
	1 ft x 1 ft x 7 mil	250	749788-1EA 749788-5EA
	1 ft x 1 ft x 7 mil	300	749818-1EA 749818-5EA
Indium tin oxide coated glass slide, square	25 x 25 x 1.1 mm	8-12	703192-10PAK
	25 x 25 x 1.1 mm	30-60	703184-10PAK
	25 x 25 x 1.1 mm	70-100	703176-10PAK
Indium tin oxide coated boro-aluminosilicate glass slide	75 x 25 x 1.1 mm	5-15	576360-10PAK 576360-25PAK
Indium tin oxide coated glass slide, rectangular	75 x 25 x 1.1 mm	8-12	578274-10PAK 578274-25PAK
	75 x 25 x 1.1 mm	15-25	636916-10PAK 636916-25PAK
	75 x 25 x 1.1 mm	30-60	636908-10PAK 636908-25PAK
	75 x 25 x 1.1 mm	70-100	576352-10PAK 576352-25PAK

MATERIALS TO DRIVE INNOVATION

Across a Variety of Applications

Energy

Electrode and electrolyte materials for batteries, fuel cells; hydrogen storage materials including MOFs; phosphors; thermoelectrics; nanomaterials; precursors for nanomaterials and nanocomposites

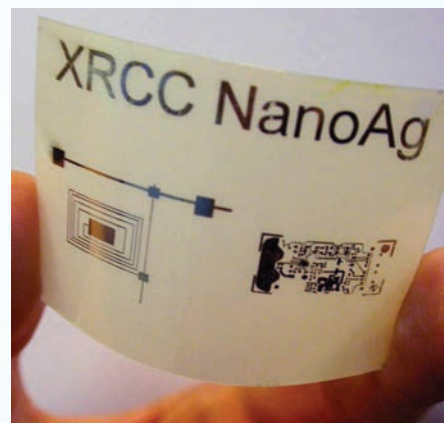
Biomedical

Materials for drug delivery, bone and tissue engineering; PEGs, biodegradable and natural polymers; functionalized nanoparticles; block copolymers and dendrimers; and nanoclays

Electronics

Nanowires; printed electronics inks and pastes; materials for OPV, OFET, OLED; nanodispersions; CNTs and graphene; precursors for PVD, CVD, and sputtering

Find more information on our capabilities at
aldrich.com/matsci



Inkjet printed silver image provided by Xerox®. We are the proud distributor of Xerox silver nanoparticle ink.

MATERIALS RESEARCH SOCIETY MID-CAREER RESEARCHER AWARD

Dr. Hongjie Dai Receives the 2016 Materials Research Society Mid-Career Researcher Award

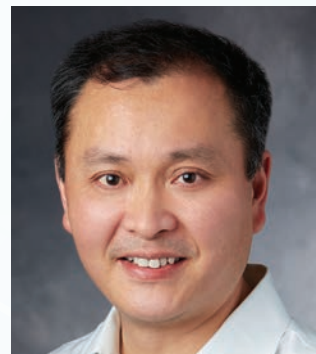
The Materials Research Society (MRS) awarded Hongjie Dai, professor of chemistry at Stanford University, the Mid-Career Researcher Award "for seminal contributions to carbon-based nanoscience and applications in nanoelectronics, renewable energy, and biological systems." The MRS Mid-Career Researcher Award, endowed by Aldrich® Materials Science, recognizes exceptional achievements in materials research made by mid-career professionals.

About Dr. Dai

Dr. Dai pioneered the controlled growth of carbon nanotubes using metal-catalyzed chemical vapor deposition, showing for the first time that high-quality single-walled nanotubes could be synthesized using a method that enables control over the growth process. He used his knowledge of nanotube growth to demonstrate hierarchical organization over multiple length scales. Dai also exploited this unique control over nanotube growth to uncover basic electronic properties of metallic and semiconducting nanotubes.

Professor Dai and his group have defined the fundamental limits of nanotube transistors. Pioneering the use of nanotubes as intracellular molecular transporters for biological molecules and cancer drugs, demonstrating that key spectroscopic properties unique to nanotubes and other carbon nanostructures make them ideal for biological detection, fluorescence imaging in the second near-infrared window, drug delivery, and cancer therapy via in vivo photothermal tumor destruction.

Hongjie Dai is the J. G. Jackson and C. J. Wood Professor of Chemistry at Stanford University. He earned his Ph.D. in applied physics/physical chemistry from Harvard University. He is the Honorary Chair Professor of the National Taiwan University of Science and Technology, a Fellow of the American Association for the Advancement of Sciences and the American Academy of Arts and Sciences, and serves on the editorial boards of eight publications. Dr. Dai has written more than 250 papers and is ranked as one of the most cited chemists (in materials chemistry) by Thomson Reuters.



Dr. Hongjie Dai

For more information, visit
aldrich.com/mrsaward

SAL
84314-517860
07-2016